

Review

Toward Dendrite-Free Deposition in Zinc-Based Flow Batteries: Status and Prospects

Zeyu Xu and Maochun Wu * 

Department of Mechanical Engineering, The Hong Kong Polytechnic University, Hung Hom, Kowloon, Hong Kong SAR 999077, China

* Correspondence: maochun.wu@polyu.edu.hk

Abstract: Safe and low-cost zinc-based flow batteries offer great promise for grid-scale energy storage, which is the key to the widespread adoption of renewable energies. However, advancement in this technology is considerably hindered by the notorious zinc dendrite formation that results in low Coulombic efficiencies, fast capacity decay, and even short circuits. In this review, we first discuss the fundamental mechanisms of zinc dendrite formation and identify the key factors affecting zinc deposition. Then, strategies to regulate zinc deposition are clarified and discussed based on electrode, electrolyte, and membrane. The underlying mechanisms, advantages, and shortcomings of each strategy are elaborated. Finally, the remaining challenges and perspectives of zinc-based flow batteries are presented. The review may provide promising directions for the development of dendrite-free zinc-based flow batteries.

Keywords: zinc-based flow battery; zinc deposition; electrode modification; electrolyte modulation; membrane engineering



Citation: Xu, Z.; Wu, M. Toward Dendrite-Free Deposition in Zinc-Based Flow Batteries: Status and Prospects. *Batteries* **2022**, *8*, 117. <https://doi.org/10.3390/batteries8090117>

Academic Editor: Claudio Gerbaldi

Received: 29 July 2022

Accepted: 1 September 2022

Published: 6 September 2022

Publisher's Note: MDPI stays neutral with regard to jurisdictional claims in published maps and institutional affiliations.



Copyright: © 2022 by the authors. Licensee MDPI, Basel, Switzerland. This article is an open access article distributed under the terms and conditions of the Creative Commons Attribution (CC BY) license (<https://creativecommons.org/licenses/by/4.0/>).

1. Introduction

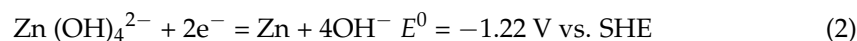
Switching from fossil fuel to renewable energy sources (e.g., wind and solar) is critical for combating climate change and energy crises [1]. Although the last few decades have witnessed significant technological advances and dramatic cost reduction in wind and photovoltaic power generation, the utilization of these renewable energy sources has been severely limited by their intermittent characteristics [2,3]. One effective solution to this challenge is to employ energy storage technologies that can store fluctuating energy sources on a large scale and supply them to the grid and end-users in a stable manner. Aqueous redox flow batteries (ARFBs) are well suited for this application because of their distinct advantages, including high safety, high efficiency, superior flexibility, and excellent scalability. Particularly, vanadium redox flow batteries (VRFBs), iron/chromium flow batteries (ICFBs), and zinc-based flow batteries (ZFBs) have achieved considerable advancement and are now on the verge of commercialization [4]. However, the high price and low solubility of vanadium species, the sluggish kinetics of chromium redox reactions, and the aging effects of chromium diminish the potential of VRFBs and ICFBs for wide commercial applications [5,6]. By contrast, ZFBs stand out as an attractive candidate for large-scale energy storage owing to their low cost, nontoxicity, high energy density, and recyclability [7–9]. A comparison between different ZFBs is presented in Table 1. In the case of zinc–bromine flow batteries, it has been shown that the practical specific energy, energy density, specific power, and power density reach $60\text{--}85 \text{ W}\cdot\text{h kg}^{-1}$ [7,10], $15\text{--}65 \text{ W}\cdot\text{h L}^{-1}$ [7], $90\text{--}110 \text{ W kg}^{-1}$ [10,11], and $4\text{--}6 \text{ W L}^{-1}$ [12], respectively. Moreover, their power rating, cycle life, and round-trip efficiency are up to 2 MW [13], 10 years, and 85% [14], with a low capital cost of $\$400 \text{ kW h}^{-1}$ [7,10]. In early 2022, a 10 kW/30 kWh zinc–bromine flow battery system for residential energy storage was developed by the Dalian Institute of Chemical Physics, Chinese Academy of Sciences [15], showing the great promise of ZFBs for industrial applications.

ZFBs are typical hybrid flow batteries that involve the plating and stripping of zinc (Zn) at the negative electrode during the charging and discharging process. As an amphoteric metal, Zn undergoes different electrochemical reactions in acidic and alkaline solutions:

In acidic or neutral solutions



In alkaline solutions



Although the electrochemical reactions seem to be simple as depicted in the equations, the real electrochemical process is much more complex, and Zn dendrites are easily formed during the charging process, posing a tremendous challenge for the development of ZFBs [16]. The formation of Zn dendrites will increase the surface area that accelerates side reactions and may detach from the electrode surface during the discharge process, resulting in low Coulombic efficiencies and rapid capacity decay [17,18]. Even worse, the rampant growth of Zn dendrites will penetrate the membrane/sePARATOR, causing short circuits in the ZFBs [19]. Therefore, it is imperative to develop an effective solution for suppressing the formation of Zn dendrites. Thus far, considerable efforts have been devoted to understanding the fundamental mechanisms of Zn dendrite formation, and various methods have been proposed to solve the problem. In general, these methods can be classified into three categories: (i) electrode modification [20–22]; (ii) electrolyte modulation [16,23–25]; and (iii) membrane engineering [26–28]. The performance corresponding to ZFBs classified by these methods is summarized in Table 2. In this review, the formation and growth mechanisms of Zn dendrites are first discussed, and the key factors affecting Zn deposition are identified and elaborated. Then, approaches to tackling Zn dendrites are summarized based on electrode, electrolyte, and membrane. Finally, the remaining challenges and application prospects of ZFBs are presented.

Table 1. Comparison of various types of ZFBs.

Media	Types	Voltage (V)	Current Density (mA cm^{-2})	Energy Efficiency (EE) (%)	Areal Capacity (mA h cm^{-2})	Cycle Number
Acid	Zn-V [29]	1.85	20	72	20	50
	Zn-Fe [30]	1.53	30	71.1	-	50
	Zn-PbO ₂ [31]	2.4	20	83	-	10
	Zn-Ce [32]	1.86	2	64	-	15
	Zn-Mn [33]	1.66	20	75	-	300
Neutral	Zn-Fe [34]	1.32	30	86.7	-	2000
	Zn-Mn [35]	1.55	40	78	20	400
	Zn-I ₂ [36]	1.38	20	70	5	600
	Zn-Br [37]	1.84	180	63.5	40	400
	Zn-TEMPO [38]	1.7	80	~52	-	1000
Alkaline	Zn-Fe [39]	1.88	80	86.8	20	120
	Zn-Ni [40]	1.70	80	77.5	25	60
	Zn-Air [41]	1.53	10	60	-	2660

Table 2. Performance comparison of ZFBs using different strategies.

Methods	Type	Electrode	Membrane	Electrolyte	Current Density (mA cm ⁻²)	Energy Efficiency (%)	Areal Capacity (mA h cm ⁻²)	Cycle Number
Electrode modification	Zn-Br [42]	NTCF	Daramic HP (~900 µm)	2 M ZnBr ₂ + 3 M KCl + 0.4 M MEPBr	80	75.91	66.6	-
	Zn-Br [21]	CZ-5	SF600 separator	2 M ZnBr ₂ + 0.5 M ZnCl ₂ + 4 M NH ₄ Cl + 0.02 M MEPBr	100	>60	20	5000
	Zn-Br [43]	SH/PH	Daramic HP (~900 µm)	2 M ZnBr ₂ + 3 M KCl + 0.8 M MEPBr	40	-	40	142
	Zn-Br [44]	Titanium mesh + carbon paper + graphite plate/carbon paper + graphite plate	Nafion 115	2.25 M ZnBr ₂ + 3 M KCl	80	34.68	10	650
Electrolyte modulation	Zn-Fe [45]	Carbon felts	PBI membrane	0.4 M Zn(OH) ₄ ²⁻ + 3 M OH ⁻ + 0.01 M THEED/0.8 M Fe(CN) ₆ ⁴⁻ + 3 M OH ⁻	80	~85.4	100	180
	Zn-I ₂ [46]	Graphite felts	Nafion 115	1 M ZnI ₂ + 1 M NH ₄ Br	40	85	40	100
	Zn-Br [23]	Graphite felt + poly-acrylonitrile felt/graphite felt	Nafion 212	2 M ZnBr ₂ + 1 M MSA	40	75	20	50
	Zn-Br [25]	Graphite electrodes	Porous separator	2.25 M ZnBr ₂ + 0.5 M ZnCl ₂ + 0.8 M MEPBr + 5 ml L ⁻¹ Br ₂ + HBr + 0.1 M CrCl ₃ ·6H ₂ O/carbon slurry	20	76.1	~85.14	-
	Zn-Ni [47]	Graphite + polyvinylidene-fluoride composite/sintered nickel plate	-	6 M KOH + 0.5 M ZnO + 5 mM TEAH	20	79	5	50
	Zn-Fe [48]	Carbon felts	Perfluorinated sulfonic acid membrane	0.5 M ZnCl ₂ + 0.05 M NAM + 3 M KCl/0.5 M K ₄ Fe(CN) ₆ ·3H ₂ O + 1 M KCl	20	83	3.33	400
	Zn-Br [24]	Carbon felts	SF600 membrane	0.5 M ZnBr ₂ + 0.125 M Zn(ClO ₄) ₂	20	71	-	25
	Zn-Br [28]	Carbon felts	Porous polyolefin/PEG composite membrane	2 M ZnBr ₂ + 3 M KCl + 0.8 M MEPBr	40	-	40	>100
Membrane engineering	Zn-Fe [49]	Carbon felts	ns-MFI-P/S-7	0.3 M Zn(OH) ₄ ²⁻ + 5 M NaOH/0.6 M K ₄ Fe(CN) ₆ + 5 M NaOH	80	81.9	13.33	600

Table 2. *Cont.*

Methods	Type	Electrode	Membrane	Electrolyte	Current Density (mA cm ⁻²)	Energy Efficiency (%)	Areal Capacity (mA h cm ⁻²)	Cycle Number
Zn-Fe [26]	Carbon felts	Turing-PBI-80		3.8 M NaOH + 0.2 M ZnO/3 M KOH + 0.4 M Na ₄ [Fe(CN) ₆] ⁴⁻ ·12H ₂ O + 0.4 M Zn(OH) ₄ ²⁻	80	90.1	160	110
Zn-Fe [50]	Carbon felts	BN-M membrane		+ 3 M OH ⁻ /0.8 M Fe(CN) ₆ ⁴⁻ + 3 M OH ⁻	80	87.6	66.67	500
Zn-Fe [51]	Carbon felts	DM-HM		0.4 M Zn(OH) ₄ ²⁻ + 3 M KOH/0.8 M Fe(CN) ₆ ⁴⁻ + 3 M KOH	80	88.3	20	500
Zn-Fe [52]	Graphite sheets	The self-made anion-exchange membrane		1 M ZnCl ₂ /0.5 M FeCl ₂ + 0.5 M FeCl ₃ + 2 M NH ₄ Cl	25	78.2	12.5	30

2. Mechanisms of Zn Dendrite Formation

Although the underlying mechanisms of Zn deposition and dendrite growth have not been fully understood, it is generally accepted that the Zn deposition process involves three steps regardless of the pH of the electrolyte: (1) liquid-phase mass transfer (Zn²⁺ ion diffusion), (2) charge transfer (Zn²⁺ ion reduction), and (3) electrocrystallization (Zn nucleation and growth) [53]. The morphology of Zn electrodeposition is determined by the nucleation and growth process. As depicted in Figure 1a, during the charging process of the ZFB, Zn²⁺ ions adjacent to the electrode interface are initially reduced to form nuclei, which results in a concentration gradient of Zn²⁺ ions between the electrode surface and bulk electrolyte [54,55]. The presence of the concentration gradient will trigger a deviation of the electrode potential from the equilibrium potential, thereby accelerating the accumulation of Zn atoms on the deposited nuclei [56,57]. It should be noted that the electrode surfaces are not always smooth and flat. As a result, Zn nuclei tend to be formed at high curvature tip protrusions, including dislocations, boundaries, and impurities, resulting in inhomogeneous Zn deposition (known as the “tip effect”) [43,54,58–60]. Under the collective effect of the concentration gradient and tip effect, Zn nuclei will gradually grow into dendrites.

It is worth noting that, although the formation of dendrites shares similar mechanisms, the exact fundamental reactions for Zn electrodeposition in alkaline and acidic/neutral electrolytes are different [53]. In alkaline electrolytes, Zn species typically exist in the form of zincate ions (Zn(OH)₄²⁻), which are reduced to metallic Zn on the surface of the negative electrode during battery charging [61], while the Zn species engaged in the reaction are Zn²⁺ ions in the neutral or slightly acidic electrolytes [62]. Note that in alkaline electrolytes, the liquid-phase mass transfer step is followed by an additional pre-transformation step, that is, the conversion of Zn(OH)₄²⁻ with the high coordination number into Zn(OH)₂ with the low coordination number as reaction species for the subsequent charge transfer [53]. This step is absent in neutral or slightly acidic electrolytes [63]. It is well acknowledged that Zn dendrites exhibit low formation barriers and grow readily in alkaline electrolytes in comparison with neutral or slightly acidic electrolytes, especially at a high operating current density [7,54,64,65]. This is because Zn presents a high electrochemical activity along with thermodynamic instability in alkaline solutions [66–68].

To reduce the Zn²⁺ ions and form a solid phase, a nucleation energy barrier needs to be overcome, as shown in Figure 1b [69]. This is typically reflected in a sharp spark of voltage at the initial stage in a voltage–time plot. After nucleation, the potential of Zn deposition gradually rises, ascribed to the continuous plating of Zn. The difference between

tip potential and subsequent stable potential is usually defined as nucleation overpotential, which has a profound effect on the size and generation rate of Zn nuclei. Of note, the effects of nucleation overpotential on Zn nucleation and growth remain elusive. Some researchers found that with higher nucleation overpotentials, the nucleation rate is faster, and the nuclei size is smaller and finer, which is conducive to uniform Zn deposition [7,70–72]. However, if the nucleation overpotential is too high, Zn^{2+} ions are more inclined to deposit on existing Zn nuclei rather than generate new nuclei on the bare electrode, leading to severe dendrite formation [73–76]. On the contrary, some results show that uniform Zn deposition is achieved when the nucleation overpotential is small [77–79]. These controversial results call for more investigations to clarify the role of overpotential in the Zn deposition process. Moreover, Zn dendrites become more severe after charge/discharge cycles. This is because Zn usually cannot be completely stripped during the previous discharge process, and the residual Zn becomes preferential nuclei for subsequent Zn deposition [80]. The accumulated non-uniform Zn residue will trigger more severe Zn dendrite formation, as displayed in Figure 1c. The intensified dendrites will eventually penetrate the membrane, leading to short circuits and thus the failure of ZFBs.

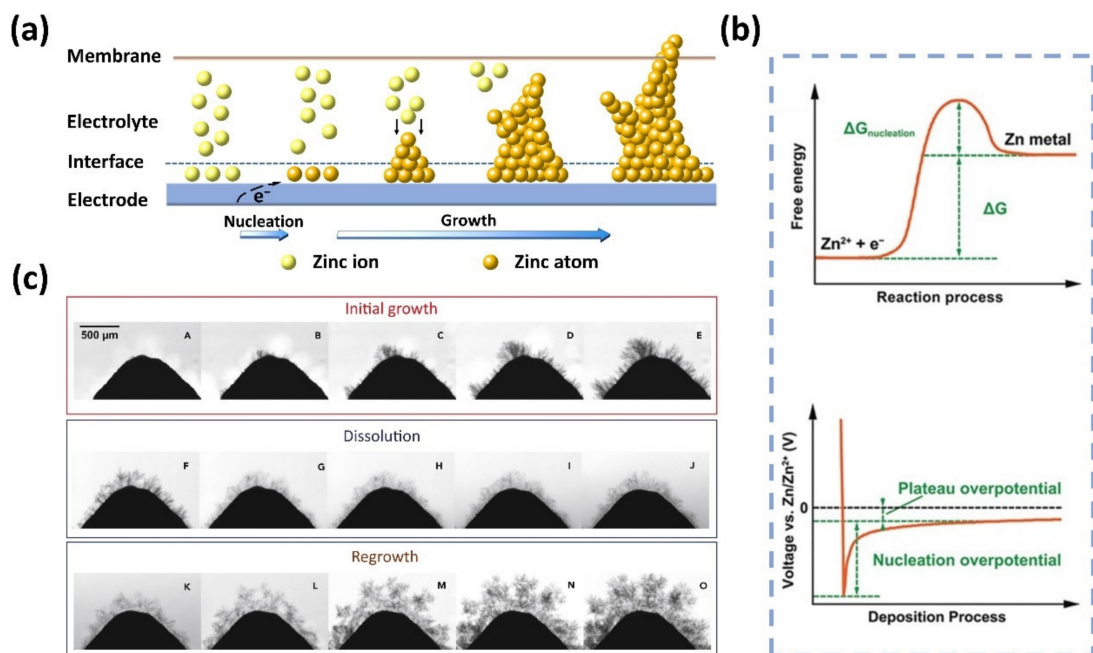


Figure 1. (a) Schematic illustration of the formation and growth of Zn dendrites. (b) The energy barrier involved in Zn nucleation and the typical voltage profile during Zn deposition. (Reproduced from [69] with permission from Wiley.) (c) The growth, dissolution, and regrowth process of Zn dendrites during battery cycling. (Reproduced from [80] with permission from Elsevier).

3. Key Factors Affecting Zn Deposition

As mentioned above, the electrodeposition of Zn is a complex process, and the evolution of Zn dendrites may be affected by various key design and operating factors. In this section, the effects of principal factors, including electrode parameters (e.g., substrates, surface properties), electrolyte composition (e.g., salts and ion concentration), flow rate, operating current density, and temperature are discussed. Adverse effects arising from Zn corrosion and hydrogen evolution reaction (HER) will also be elaborated.

3.1. Effect of Electrode

Electrodes play a crucial role in determining the electrochemical performance of Zn as they not only provide active sites for Zn^{2+}/Zn redox reactions but also a place for Zn deposition. Therefore, the properties of electrodes will impose a significant impact on the Zn electrodeposits and thus the battery performance. For example, electrocatalytic

activity and electrode surface area usually determine the activation loss, nucleation, and subsequent Zn growth. The pore structure of the electrode will affect the transport and distribution of electrolytes that will influence the Zn deposition process. Other parameters such as electrical conductivity, thickness, hydrophilicity, mechanical strength, and chemical stability will also affect the efficiency and cyclability of ZFBs.

Generally, the Zn electrodes can be divided into two types, i.e., planar and porous. For the plate electrode, a gap is reserved between the electrode and membrane for Zn deposition and electrolyte flow. The distance of the gap is a key parameter that needs to be optimized for this type of electrode as it has a direct effect on the areal capacity and internal resistance. However, due to the low active surface area and severe dendrite growth of plate electrodes, more attention has been shifted to porous electrodes, in particular, porous carbon electrodes with attractive features, including large specific surface area, high porosity, good chemical/electrochemical stability, and low cost. More importantly, it should be noted that the capacity of ZFBs is determined by the electrodeposited Zn at the negative electrode during charge.

3.2. Effect of Electrolyte Composition

A typical electrolyte for ZFBs consists of Zn species in an aqueous solution with or without supporting electrolytes and additives. Based on the pH of electrolytes, ZFBs can be divided into alkaline and neutral/acidic flow batteries. In alkaline ZFBs, the active species is $\text{Zn}(\text{OH})_4^{2-}$ while KOH, NaOH, and LiOH usually serve as supporting electrolytes. The types of supporting electrolytes and concentrations will influence the electrolyte conductivity, solubility of zincate ions, and electrochemical performance of Zn electrodes. For instance, it was found that a 6 M concentration of KOH enables a Zn-Ni flow battery to achieve the highest Coulombic efficiency, but the high concentration of KOH suppresses the reduction of Zn^{2+} ions by limiting their transport to electrodes [81]. Due to the severe corrosion and dendrite growth, additives are usually added to the electrolytes to improve the performance. The effects of additives will be discussed in Section 4.2.

In the neutral/acidic electrolytes, various Zn salts can be used, such as ZnCl_2 , ZnBr_2 , ZnI_2 , $\text{Zn}(\text{CH}_3\text{SO}_3)_2$, $\text{Zn}(\text{ClO}_4)_2$, and ZnSO_4 . The Zn electrochemistry will be affected by the type of anions and concentration of Zn^{2+} ions. For example, it is reported that dendrites are less likely to form in the acidic $\text{Zn}(\text{CH}_3\text{SO}_3)_2$ electrode due to the complexation of Zn^{2+} and CH_3SO_3^- anions [82]. Kim and Jeon found that the presence of $\text{Zn}(\text{ClO}_4)_2$ in ZnBr_2 electrolyte improved the Zn dissolution rate compared with conventional ZnCl_2 [24]. Similar to alkaline electrolytes, supporting electrolytes and additives also have significant effects on the performance of Zn electrodes. Rajarathnam et al. compared the influence of different sodium salts with anions of Cl^- , Br^- , SO_4^{2-} , H_2PO_4^- and NO_3^- on the Zn electrode of Zn-Br flow batteries [83]. It was found that the addition of NaBr , Na_2SO_4 , and NaH_2PO_4 could improve the electrochemical performance of Zn electrodes.

The concentration of Zn^{2+} ions also has a strong influence on the Zn deposition characteristics [84]. It is revealed that, at high concentrations of Zn^{2+} ions (≥ 0.4 M), the Zn nuclei deposited at the interface undergo rapid growth in an instantaneous mode [85]. The formed Zn crystals will preferentially expose the thermodynamically stable (002) crystal plane. The plane grows parallel to the substrate and eventually forms the dense and flat block. By contrast, nucleation will turn into a progressive mode when the concentrations of Zn^{2+} ions are low (≤ 0.3 M). The generated crystals are haphazardly distributed and eventually form a disorganized mossy shape, which will drive the formation and growth of Zn dendrites. Therefore, the electrolyte used in ZFBs typically has a Zn^{2+} ion concentration of 2 M during the initial plating stage, and an excessive amount of electrolyte is employed to ensure that the concentration of Zn^{2+} ions is greater than 0.4 M at the end of the plating process [28,37,85–87].

3.3. Effect of Flow Rate

Because inhomogeneous ion distribution is one of the major factors that result in dendrite growth, employing flowing electrolytes is an effective strategy for facilitating mass transport and thus suppressing Zn dendrite formation [88]. Under convection, Zn deposition reactions exhibit fast kinetics resulting from increased limited current densities [89,90]. Moreover, relatively slow reaction kinetics for Zn oxidation is also enhanced with an increase in mass transfer rate [89]. As a result, ZFBs are capable of operating at higher current densities than their static counterparts. Previous experimental results suggest that a small flow rate of 2 cm s^{-1} can significantly improve the morphology of Zn deposition [7]. As the flow rate rises, the Zn^{2+} ions distributed at the electrode/electrolyte interface become more uniform, and the width of the Nernst diffusion layer becomes thinner [7]. When the electrolyte flow rate is up to 15 cm s^{-1} , the direction of Zn deposition will bend along the flow direction, which minimizes the possibility of short circuits [91]. However, high flow rates will increase the pressure drop, leading to additional energy loss and even leakage of the electrolyte. Therefore, the flow rate needs to be finely regulated to find a balance between Zn dendrites and pressure drop. Moreover, Zn dendrites may still be formed when ZFBs are cycled for long periods and at high current densities, especially in an alkaline solution. More efforts are needed to understand the coupled fluid flow, mass transport, and solid-phase evolution in the porous media.

3.4. Effect of Current Density

Current density is one of the critical indicators for evaluating the performance of flow battery systems. Increasing the current density can raise the power density and reduce the operating cost of flow batteries, thus accelerating the promotion of flow batteries in the energy storage market. Unfortunately, ZFBs usually need to be operated at low current densities ($<120 \text{ mA cm}^{-2}$) [92–94] in comparison to the full-flow systems (e.g., VRFBs and ICFBs), which are capable of operating at high current densities ($>200 \text{ mA cm}^{-2}$) [95–97]. One of the prime reasons is that the growth of dendrites is exacerbated at high current densities, which will cause the failure of ZFBs. At high current densities, a large concentration gradient of Zn^{2+} ions is developed between the electrode interface and the bulk electrolyte because the mass transfer rate of Zn^{2+} ions is much lower than their reaction rate, driving the rampant growth of Zn dendrites. Therefore, a ZFB is commonly operated at low current densities, especially in practical applications [98]. Identifying an effective approach to addressing the issue of rapid dendrite growth at high current densities will significantly facilitate the widespread application of ZFB systems.

3.5. Effect of Temperature

Temperature has distinct effects on the properties of the electrolyte, including viscosity, density, and conductivity, as well as the reaction kinetics [99–102]. Theoretically, when the operating temperature rises, the nucleation overpotential of Zn^{2+} ions diminishes, and the diffusion of Zn^{2+} ions on the electrode interface is accelerated [103,104]. That is, the elevated temperature promotes the nucleation and growth process of Zn. Because of the fast diffusion behavior of ions at a high temperature, the nucleus size is more extensive, and the nucleus density is lower than that at a low temperature [105]. As the deposition process proceeds, large and sparse nuclei progressively grow, and the neighboring nuclei fuse to produce dense deposition layers [106]. In contrast, the low temperature makes the electrolyte viscosity increase and the mobility of ions sluggish, which induces the deposition of ions on the nucleation sites. Unavoidably, further deposition of nuclei predisposes to the overlapping of nuclei and the evolution of dendrites [106]. Therefore, the fast ion diffusion rate at a high temperature prevents Zn dendrite formation. In practice, however, the high temperature will exacerbate parasitic reactions, such as hydrogen evolution and Zn corrosion [107–109]. In addition, the self-discharge behavior caused by active species crossover from the positive electrode is worsened at a high temperature [110]. These adverse effects associated with high temperature reduce the Coulombic efficiency of ZFBs

and affect the efficient use of the electrolyte. At present, investigations on the thermal characteristics of ZFBs are relatively limited, rendering it challenging to optimize the temperature for ZFBs.

3.6. Effect of Parasitic Reactions

Owing to the low redox potential of the Zn^{2+}/Zn reaction, Zn is thermodynamically unstable in aqueous electrolytes. Consequently, parasitic reactions such as HER and Zn corrosion frequently occur during Zn deposition processes. In practice, the HER process is relatively complex since it is influenced by various factors such as temperature, applied voltage, surface roughness of electrodes and electrolyte composition [61,111]. The occurrence of hydrogen evolution will generate bubbles which will cause an uneven electric field distribution and trigger Zn dendrite growth. Even worse, the formation of dendrites can supply more reaction sites for hydrogen evolution, exacerbating its progress [112]. Strategies such as electrode modification and adding additives have been proposed to suppress HER. Subject to the pH of the electrolyte, the hydrogen evolution overpotential of 1.0 V can be achieved by using organic additives and inert materials with high HER overpotentials [113]. Nevertheless, some organic additives that significantly suppress HER are composed of hydrocarbon chains with large molecular weights or long lengths, which may strongly adsorb on the reactive sites, thus slowing down the charge transfer process of Zn^{2+} ions [107,114]. Developing an effective strategy to address the problem of hydrogen evolution remains an urgent challenge.

Accompanying HER is the spontaneous reaction between Zn and the electrolyte, which is known as Zn corrosion, posing an additional challenge for the practical application of Zn electrodes. Typically, high rates of Zn dissolution and HER will be noted in acidic electrolytes. However, at a high acid concentration (e.g., methanesulfonic acid > 6 M), the dissolution rate may slow down, resulting from the decreased availability of dissociated H^+ in the electrolyte [109]. When the pH range is 1–4, Zn corrosion and HER prefer to proceed simultaneously at mixed potentials. The Zn corrosion rate is jointly determined by cathodic control and HER kinetics [115]. In a neutral system, the H_2O in the electrolyte acquires electrons from the dissolved Zn to produce hydrogen and OH^- [116]. The accumulating OH^- will interact with Zn^{2+} ions to produce side products such as $Zn(OH)_2$ and ZnO on the electrode surface [117,118]. In alkaline solutions, the corrosion products are also ZnO and $Zn(OH)_2$ due to OH^- enrichment. Notably, the corrosion products exist in a loose structure, which fails to form an effective dense barrier to prevent further corrosion [111]. In addition, the interphase impedance incurred by corrosion products limits electron transport and ion diffusion, thereby increasing the energy barrier for Zn deposition [119–121]. Meanwhile, accumulated Zn deposition tends to occur in areas that have not yet been passivated, resulting in the formation of severe dendrites in localized regions of the electrode.

Previous works have shown that the corrosion rate is closely related to the morphology of Zn deposition and the major crystalline surface exposed [122]. Closely packed crystal planes, such as hexagonal close-packed (hcp) Zn (002) planes, have a trend towards higher corrosion resistance [123–127]. In addition, deposited layers with finer crystal sizes possess higher resistance to corrosion [128–131]. Organic and inorganic additives generally modify the morphology of Zn electrodeposits and endow electrodeposits with superior corrosion resistance [132–137]. Beyond improving the morphology of Zn, some electrolyte additives such as bismuth and indium can act as corrosion inhibitors [47,138–140]. Nonetheless, the equilibrium potential of these metal additives is close to that of Zn. Once these additives are reduced and covered by the deposited Zn, they will stop functioning in inhibiting side reactions. It should be acknowledged that HER and Zn corrosion usually occur with Zn dendrites, further complicating the process. Luckily, addressing one issue can normally alleviate other issues.

4. Strategies for Dendrite Suppression

Over the past several decades, considerable efforts have been devoted to tackling the challenges of Zn dendrites in ZFBs. The strategies can be classified based on the key components (electrode, electrolyte, and membrane) in ZFBs, as illustrated in Figure 2. In this section, we will discuss in detail the development of electrode modification, electrolyte modulation, and membrane engineering to address Zn dendrites. The underlying mechanism of each approach will also be elaborated.

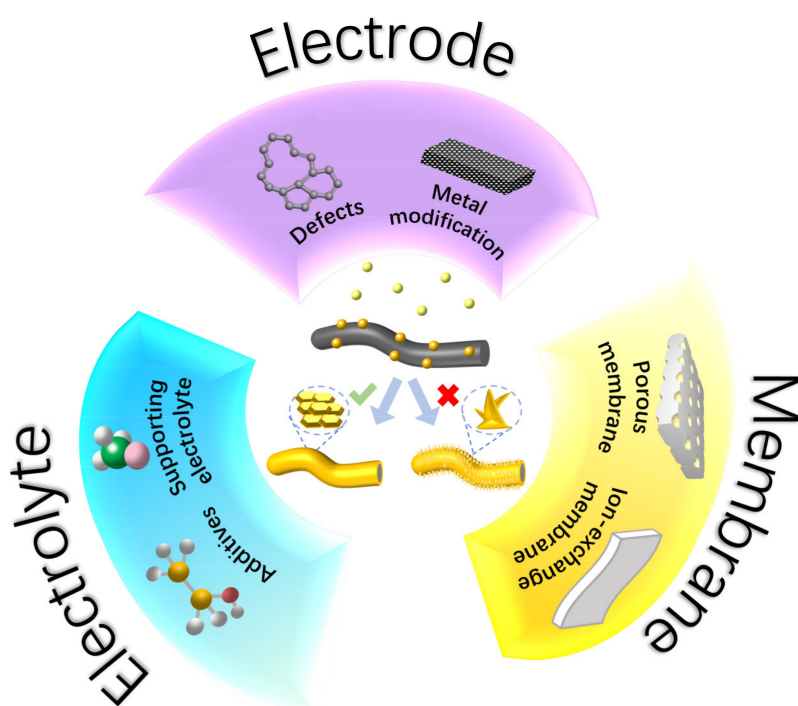


Figure 2. Electrode, electrolyte, and membrane materials for a dendrite-free ZFB.

4.1. Electrode Modification

As mentioned in Section 3.1, porous carbon fiber electrodes (e.g., carbon/graphite felt) have gained the most attention for ZFBs due to their high porosity, low cost, high stability, and broad operating potential range. The use of three-dimensional porous electrodes can reduce the local current density and provide abundant nucleation sites for Zn deposition. As a consequence, dendrite formation is mitigated, and the cycling performance of the Zn electrode is enhanced. However, it is found that Zn tends to preferentially deposit near the electrode/membrane interface, which not only restricts the areal capacity but poses a risk of penetrating the membrane due to the non-uniform Zn deposition. To unravel the effect of surface properties on Zn nucleation and growth and efficiently promote the uniform deposition of Zn on fiber surfaces, Zhao et al. investigated the adsorption and diffusion of Zn atoms on typical carbon surfaces, including the raw graphite (0001) surface, as well as surfaces with single vacancy, double vacancy and oxygen functional groups by performing first-principles calculations, as shown in Figure 3a [20]. It was found that the surface with single vacancy exhibits a remarkable anchoring effect on Zn atoms, resulting from the availability of unpaired electrons on unsaturated carbon atoms. In contrast, the remaining defects, including the surface with double vacancy and surfaces with oxygen functional groups, present weak adsorption of Zn atoms owing to the lack of unpaired electrons. Notably, Zn atoms anchored by the single vacancy defects will constitute the nucleation sites for the subsequent deposition because of the high energy barriers for Zn atom diffusion from the single vacancy. Hence, the deposition process of Zn can be adjusted by varying the content of the single vacancy on the negative electrode, thus avoiding the appearance of Zn dendrites during the charging process of ZFBs. Subsequently, defect-rich

negative electrodes were fabricated through heat-treating graphite felts in ambient air. Physical and electrochemical characterizations demonstrated that the uniform deposition of Zn atoms was achieved on thermally treated graphite felts (Figure 3b), which offers a new approach to designing dendrite-free ZFB electrodes. Subsequently, Kim et al. adopted the zeolitic imidazole framework-8 (ZIF-8) as a template to deeply investigate the effect of single vacancy carbon defects on Zn deposition, as displayed in Figure 3c [21]. The defective carbon layer is constructed via carbonizing ZIF-8 at 1000 °C. As a result of the strong hybridization effect between the s p d orbitals of Zn and the s p orbitals of single vacancy defects, the surface diffusion of Zn atoms and thus the aggregative growth of Zn is effectively hindered. The authors then employed ex situ high-angle annular dark-field scanning transmission electron microscopy and energy-dispersive spectroscopy mapping analyses to confirm that the defects facilitate Zn nucleation and growth. With well-designed defective carbon layers, the newly designed electrodes enable a Zn-Br flow battery to stably operate for 5000 cycles at a high current density of 100 mA cm^{-2} and a high area capacity of 20 mAh cm^{-2} .

Alternatively, Lu et al. demonstrated that constructing nitrogen-rich defects on carbon felts is also an effective strategy to achieve uniform Zn deposition [42]. In the study, their density functional theory calculations reveal that the defects loaded with pyridine- and pyrrole-N present strong adsorption of Zn atoms. During the charging process, reduced Zn atoms are preferentially deposited in the defects, leading to the uniform Zn deposition on the fiber surface (Figure 3d). It is shown that the ZFB with rich N-containing functional groups delivers a Coulombic efficiency of 97.25% at an ultra-high current density of 180 mA cm^{-2} . Furthermore, the Zn symmetry flow battery exhibits a long cycle of over 140 times at an area capacity of 40 mAh cm^{-2} and a current density of 80 mA cm^{-2} . It is worth noting that the introduction of defects may also alter the surface roughness (specific surface area), hydrophobicity, and electrical conductivity. The improvement in Zn deposition is the collective consequence of treatment, and it is quite challenging to distinguish the contribution of each factor. Further systematic investigations of the effect of other properties on Zn deposition are needed to gain a comprehensive understanding of the Zn deposition process.

Apart from defect engineering, modifying the electrode surface with metal nanoparticles is also a promising option for suppressing dendrite formation. Li et al. used a magnetron sputtering technique to deposit tin layers on fiber surfaces, as depicted in Figure 4a [43]. The deposited tin layers enable uniform Zn deposition as a synergistic result of sufficient Zn nucleation sites, high HER energy barrier, and minor Zn deposition overpotential (Figure 4b). However, the high production cost restricts the practical applications of the strategy. Daoud et al. used an impregnation–thermal treatment strategy to construct indium-modified layers on the electrode surface [139]. It was found that the Zn nucleation potential of modified electrodes is positively shifted by 65 mV, indicating more favorable Zn deposition on the surface of the indium-modified electrode. Moreover, the presence of indium greatly reduces HER and thus leads to higher Coulombic efficiencies of the battery. More importantly, the morphology of Zn deposited on the modified electrodes displays no nodules or dendrites. After 340 cycles of the battery, energy-dispersive X-ray spectrophotometer analysis of the modified surface demonstrates the appearance of indium, indicating the tight adhesion of indium on the modified electrode. Kim et al. investigated 3D titanium meshes as spacers to suppress the growth of Zn dendrites [44]. The three-dimensional titanium interlayer provides extra sites for Zn redox reactions and substantial electrolyte transport channels, thus enhancing the reaction kinetics and suppressing Zn dendrite growth, as seen in Figure 4c. It was demonstrated that the energy efficiency (EE) of the battery with a titanium interlayer is 14.7% higher than that of the original battery at a high current density of 80 mA cm^{-2} , confirming the practicality of the titanium mesh as an interlayer for ZFBs. Although the metal-modified layer can greatly alleviate the formation of Zn dendrites, some metals are corroded by the reaction with H^+ or crossover species

from the positive electrodes. Therefore, it is imperative to develop metal-modified layers that enable the suppression of Zn dendrite formation with high stability and durability.

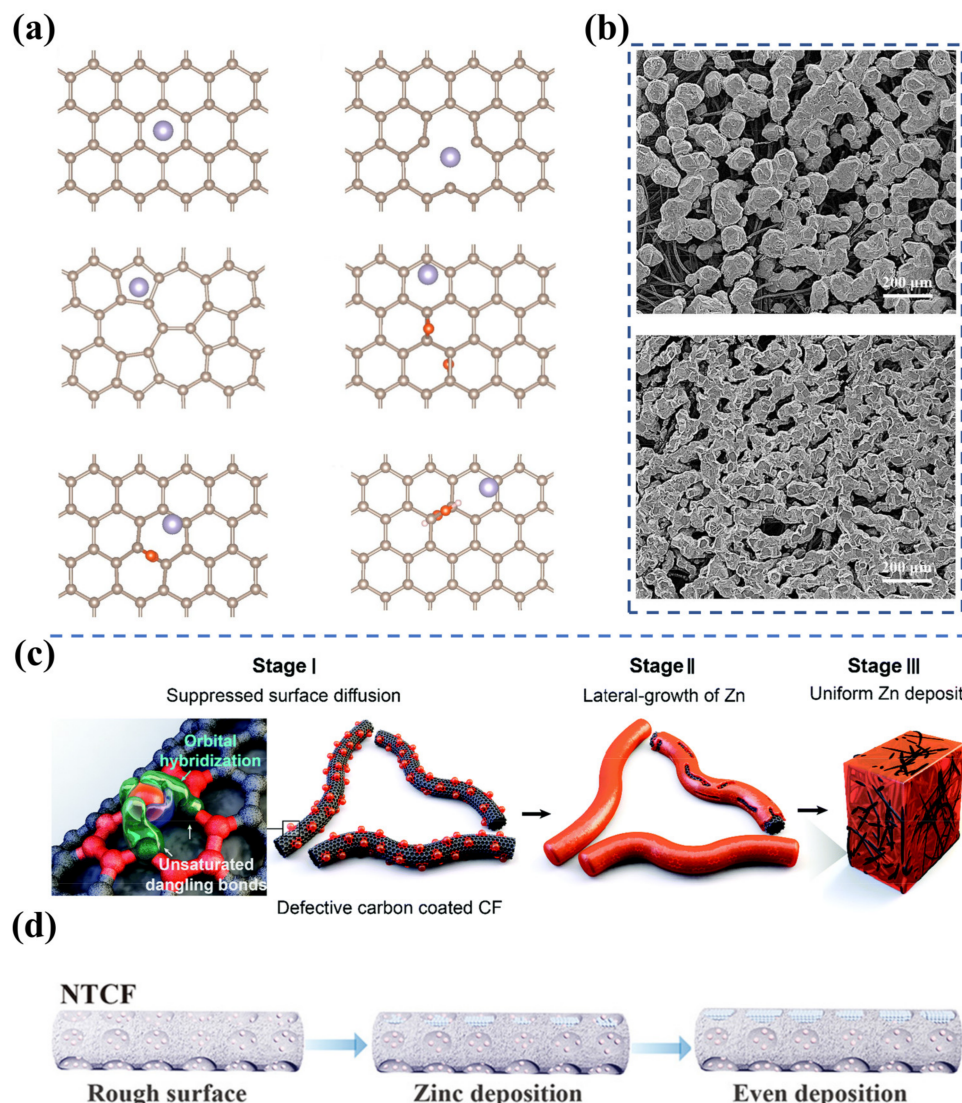


Figure 3. (a) The most stable structural morphologies of Zn atoms adsorbed on the original graphite (0001) surface, and surfaces with single vacancy, double vacancy, and oxygen functional groups. (b) SEM images of Zn deposition on pristine graphite felt (above) and heat-treated graphite felt (below) near the membrane side after charging. (Reproduced from [20] with permission from Elsevier.) (c) Schematic diagram for uniform Zn nucleation and growth on the defective layer coated electrode. (Reproduced from [21] with permission from Royal Society of Chemistry.) (d) The process of Zn deposition on the carbon felts with nitrogen-rich defects during battery charging. (Reproduced from [42] with permission from Wiley).

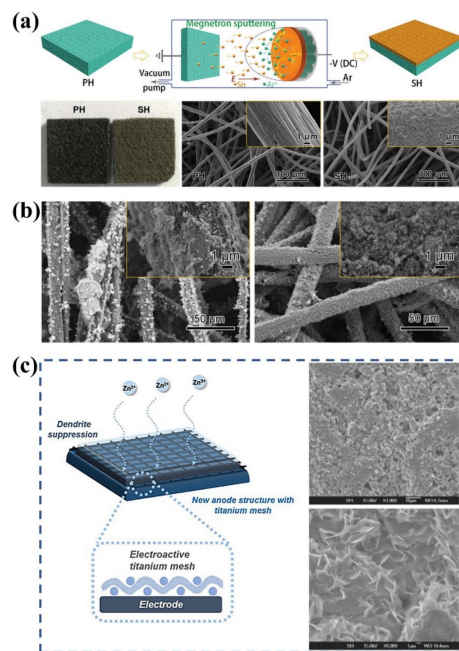


Figure 4. (a) Schematic diagram for the fabrication process of tin-modified electrodes, the morphologies of the pristine carbon felt (PH) and the tin-modified carbon felt (SH). (b) SEM images of the pristine carbon felt (left) and the tin-modified carbon felt (right) after charging. (Reproduced from [43] with permission from Wiley.) (c) Schematic diagram of the electrode with titanium mesh and SEM morphologies of the electrode with (top right) and without (bottom right) titanium mesh after initial Zn deposition. (Reproduced from [44] with permission from Nature).

4.2. Electrolyte Modulation

In general, variations in electrolyte composition will change the solvation structure of Zn^{2+} ions, the electrode/electrolyte interface, ionic conductivity, and diffusion processes of ions, thereby playing a pivotal role in determining the Zn deposition process [141–143]. Hence, it is possible and, in fact, effective to suppress Zn dendrite growth via modulating the electrolyte. The basic components of the electrolyte for ZFBs include Zn species, supporting electrolyte, additives, and water solvent. As for a specified ZFB, Zn species are usually fixed. The supporting electrolyte and additives are therefore added to tune the electrolyte properties. Currently, sodium chloride and potassium chloride are the most widely used supporting electrolytes in near-neutral electrolytes [144–147]. Although these chloride salts can improve the electrolyte conductivity, they are not favorable for Zn deposition as dendrites are usually reported in these electrolytes [19,43]. Alternatively, Wu et al. reported that methanesulfonic acid (MSA) acts as a supporting electrolyte to suppress the growth of Zn dendrites [23]. As shown in Figure 5a, much more uniform Zn deposition without dendrite growth is achieved in the presence of MSA, which is due to the complexation between Zn^{2+} cations and MSA^- anions. The same group also developed NH_4Br as a tri-functional electrolyte for Zn-I₂ flow batteries, i.e., enhancing the ionic conductivity, unlocking the capacity of iodine, and suppressing dendrite growth [46]. As displayed in Figure 5b, Zn^{2+} ions adsorbed on the electrode surface will first be reduced to form initial nuclei on the electrode surface during the nucleation process. Subsequently, a disturbed electric field around protuberances will induce continuous diffusion of Zn^{2+} ions toward the tips, resulting in severe dendrites in the bare ZnI₂ electrolyte. By contrast, the complexation effect of NH_4^+ ions will induce more uniform Zn nucleation on the surface. After being reduced, the NH_4^+ will be released and electrostatically accumulate around the tips of protuberances, forming an electrostatic shield to repel the Zn^{2+} to adjacent regions of the electrode, thereby leading to uniform, dendrite-free Zn deposition. Furthermore, Zn perchlorate can also be employed as an efficient supporting electrolyte to mitigate the growth of Zn dendrites by accelerating the dissolution rate of Zn [24]. The effect

comparison is displayed in Figure 5c. These results demonstrate that tuning the supporting electrolyte is a promising way to boost the reversibility of Zn electrodes. However, it should be noted that as the supporting electrolyte is usually used in a large amount, the developed electrolyte should be low-cost, non-toxic, and abundant.

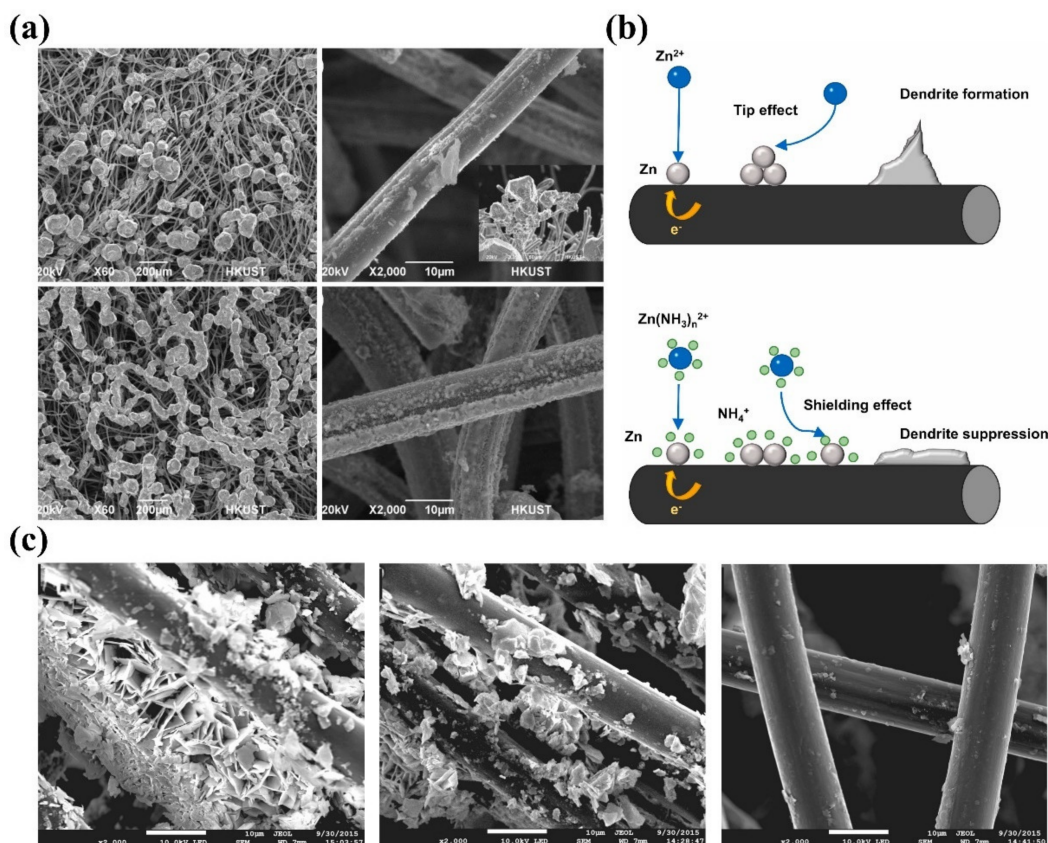


Figure 5. (a) SEM images of deposited Zn on graphite felts adjacent to the membrane side without MSA (upper images) and with 1 M MSA (lower images). (Reproduced from [23] with permission from Elsevier.) (b) Schematics of Zn^{2+} ion diffusion and deposition processes on electrodes without (upper image) and with (lower image) NH_4Br support electrolyte. (Reproduced from [46] with permission from Elsevier.) (c) SEM images of the carbon felt after 25 charge/discharge cycles with the original (left), Zn chloride (middle), and Zn perchlorate (right) support electrolytes. (Reproduced from [24] with permission from Wiley).

In addition to the supporting electrolyte, the employment of additives is a widely adopted approach to overcoming challenges facing Zn electrodes. Generally, the additives are classified into polymers, organic molecules, and metal ions [76]. Compared with supporting electrolytes, additives are usually added with a small amount. Polymers with high molecular weight selectively adsorb on the electrode surface, thus promoting uniform Zn nucleation and preventing dendrite formation. However, the overpotential of Zn deposition is increased as the active sites are blocked [107,148,149]. For example, Akolkar et al. investigated the effects of polyethylene glycol (PEG)-200 and polyethylenimine (PEI) on the suppression of Zn dendrites [149,150]. The results show that the adsorption of polymers on electrode surfaces lowers the exchange current density and increases the overpotential for Zn deposition. Notably, the adsorption strength of polymers on electrode surfaces needs to be considered. If the adsorption strength of polymers is weak, there is little effect for Zn dendrite suppression. Conversely, if polymers are strongly adsorbed onto the electrode, the Zn nucleation sites will be firmly occupied, leading to a dramatic increase in the activation polarization of ZFBs and thus a decrease in charging/discharging performance [57,76].

Therefore, exploring polymers with suitable adsorption capacity is crucial to balancing ZFB polarization and Zn dendrite formation.

Organic molecules are another promising additive for Zn dendrite suppression [151–154]. Like polymers, they tend to preferentially absorb on the electrode surface and facilitate uniform Zn nucleation at the sacrifice of overpotential. In addition to this role, organic molecules can partially replace the water in the Zn^{2+} solvation shell, which reduces the solvate water molecules and thus mitigates parasitic reactions [57]. Wang et al. investigated the use of ethanol as an additive for Zn dendrite suppression. It was shown that ethanol can be complexed with Zn^{2+} ions, alleviating the continuous growth of Zn dendrites [16]. Tang et al. used nicotinamide (NAM) as an organic molecular additive for $Zn-I_2$ flow batteries to achieve a highly reversible plating/stripping of Zn while suppressing HER [48]. Experimental characterization and theoretical calculations demonstrate that the carbonyl and amino polar groups of NAM have distinct interactions with the electrode surface. This enables NAM to adsorb on the deposited Zn layer to modulate the Zn^{2+} diffusion and avoid adverse tip effects, thus achieving uniform Zn deposition (Figure 6a) and suppressed HER. As a result of the synergistic modulation of solvation structures and electrode interfaces, the Zn-Fe flow battery displays an energy efficiency of 70% at 50 mA cm^{-2} and a high power density of 185 mW cm^{-2} .

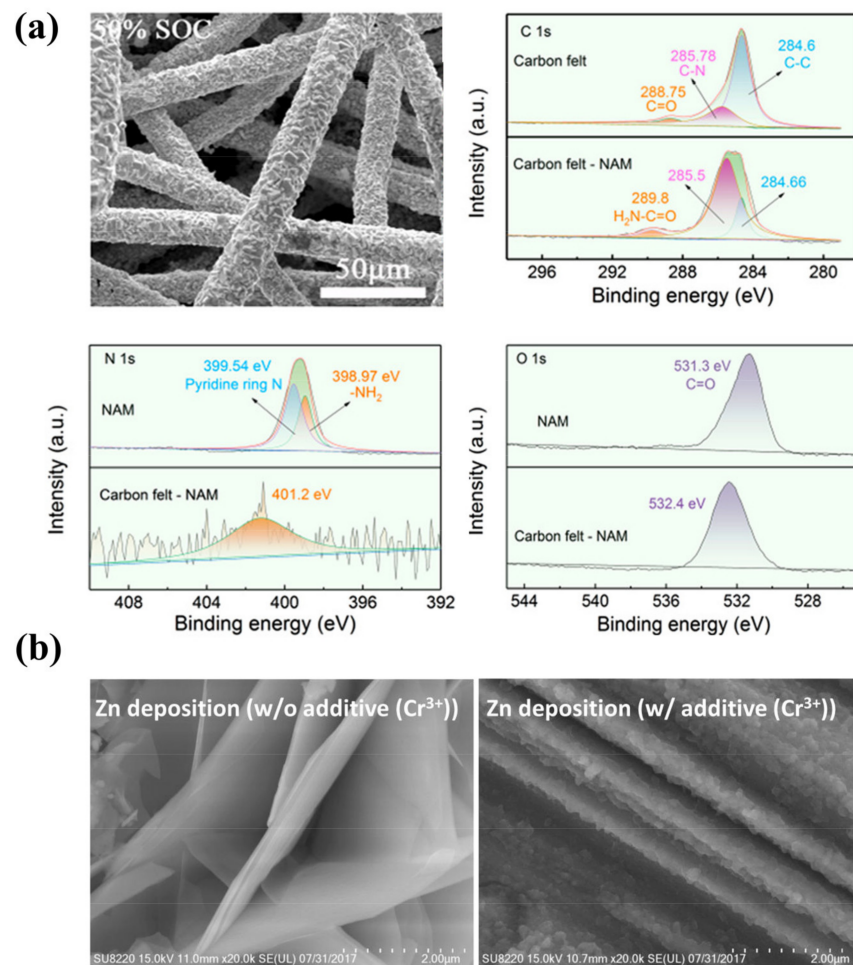


Figure 6. (a) The morphology of the Zn plated on carbon felts after the addition of NAM and the high-resolution XPS of the corresponding samples. (Reproduced from [48] with permission from American Chemical Society.) (b) Morphologies of Zn electrodeposited on graphite felts without Cr^{3+} (left) and with 0.1 M of Cr^{3+} (right). (Reproduced from [25] with permission from Elsevier).

Metal cations with reduction potentials between the Zn^{2+} ion reduction potential and the hydrogen evolution potential can be used as additives to address the Zn dendrite

issue [155]. They preferentially absorb on the tips without being reduced and form an electrostatic shielding layer impeding the continuous deposition of Zn^{2+} ions, thus suppressing the growth of Zn dendrites [156]. Based on this principle, Kim et al. demonstrate that adding Cr^{3+} can transform the deposited layers from needle-like dendrites to mirror-image films and shift the growth direction of Zn from the vertical to the horizontal plane (Figure 6b) [25]. As a result, the Coulombic efficiency of the ZFB increased from 89.8% to 91.3% after the addition of Cr^{3+} ions.

Although various additives have been investigated for suppressing Zn dendrite growth, they mainly function at low capacity and low current density. Moreover, they suffer from degradation upon cycling. The mechanisms underlying the decay remain unclear and require more investigations. Given its simplicity, electrolyte modulation will continue to be one of the most promising strategies to address the Zn dendrite challenge. It can be envisioned that the advances in theoretical calculations will accelerate the discovery of more effective additives.

4.3. Membrane Engineering

Unlike conventional all-liquid flow batteries, membranes in ZFBs are at risk of being penetrated by the growing Zn dendrites. Therefore, the membrane should have sufficient mechanical strength apart from high chemical stability, high ion selectivity, good ionic conductivity, and low cost. Typically, the membranes employed in ZFBs are categorized into two types: ion-exchange membranes and porous membranes. Perfluorosulfonic acid membranes (e.g., Nafion membranes) with superior mechanical strength and chemical stability are the most widely used in the lab-scale ZFBs [46,48,157–159]. However, the high membrane resistance and production cost limit their commercial-scale application. To overcome these challenges, Li et al. prepared an inexpensive and stable ion-exchange membrane made of sulfonated poly (ether ether ketone) (SPEEK) [160]. The membrane was synthesized on a pilot scale (Figure 7), and it was demonstrated that a ZFB stack (4000 W) with this membrane can be operated continuously for more than 800 h. These results indicate that the prepared pilot-scale SPEEK membranes hold great potential for ZFB applications.

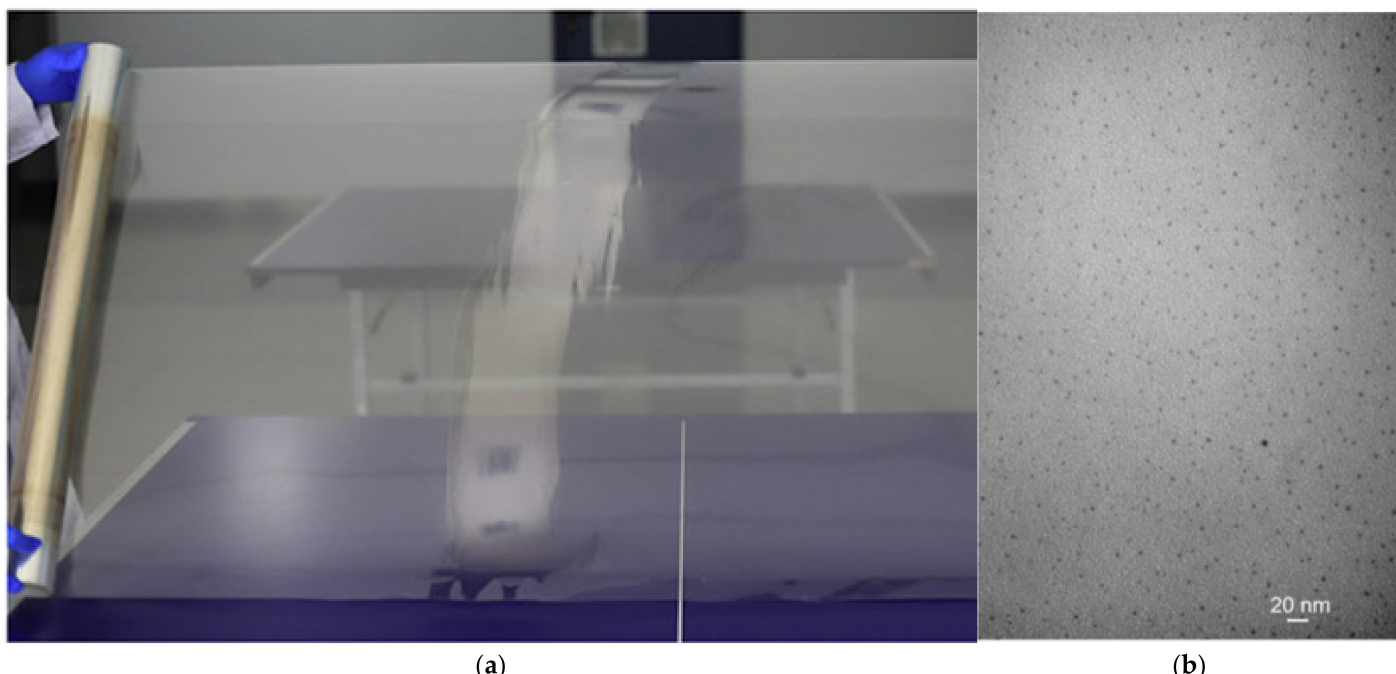


Figure 7. (a) Macroscopic morphology and (b) microscopic morphology of pilot-scale SPEEK membrane. (Reproduced from [160] with permission from Elsevier).

Compared with ion-exchange membranes, porous membranes can usually be fabricated at a lower cost. Moreover, they exhibit a higher ionic conductivity, which is conducive to high-power ZFBs. Hence, developing porous membranes with excellent dendrite suppression capability is of great significance for ZFBs. Several attempts have been made to achieve this objective [19,28,50,161–163]. Li et al. fabricated a novel composite membrane by coating polyethylene glycol (PEG) on the surface and pore walls of a porous polyolefin membrane [28]. The PEG coating as an ionic conductor promotes the uniform distribution of Zn^{2+} concentration. Meanwhile, the PEG coating also works as a passivation layer for Zn atoms, enabling a uniform electric field distribution on the negative electrode surface. As a consequence of the dual-functional design, uniform Zn deposition without obvious dendrites is achieved, as demonstrated in Figure 8a. In addition, the same group also developed a boron nitride nanosheet (BNNS)/porous poly (ether sulfone) (PES) composite membrane [50]. It is reported that BNNSs with high thermal conductivity function as a heat-porter to improve the temperature distribution on electrode surfaces, thus converting the deposited Zn from needle-like to French fries-like morphology, as shown in Figure 8b. Meanwhile, the high mechanical strength of BNNSs prevents the damage from the deposited Zn. As a result, an alkaline Zn-Fe flow battery assembled with the composite membrane is capable of running for 500 cycles at 80 mA cm^{-2} . Although promising results in Zn dendrite suppression have been achieved via membrane engineering, research in this direction is still limited compared with electrode modification and electrolyte modulation. However, given the important role of membranes, more efforts should be devoted to developing advanced membranes to achieve high-performance ZFBs.

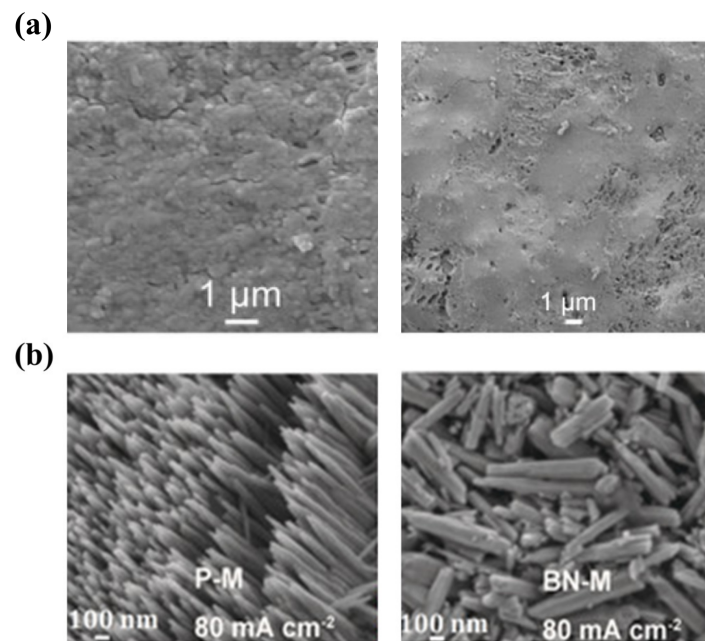


Figure 8. (a) The morphology of the porous polyolefin/PEG composite membrane (left) and Zn deposition morphology on the anode when the ZFB was assembled with the membrane (right). (Reproduced from [28] with permission from Elsevier.) (b) The morphologies of Zn deposition corresponding to the absence (left) and presence (right) of BNNSs in PES membranes. (Reproduced from [50] with permission from Wiley.).

5. Concluding Remarks and Outlook

In summary, the mechanisms of Zn dendrite formation, key factors affecting Zn deposition, and recent advances in addressing Zn dendrites are summarized and discussed in this review. To further advance this technology and eventually realize the commercial application of ZFBs, future efforts should be devoted to the following key issues:

1. The currently demonstrated area capacity of deposited Zn is still relatively low. This is because dendrites become more severe at a higher areal capacity. Therefore, future works need to develop Zn electrodes that can operate at a high areal capacity without dendrite growth. Engineering porous electrodes (e.g., pore size, pore distribution, surface properties) to achieve uniform Zn deposition within the porous structure would be a promising approach.
2. The underlying mechanisms of Zn deposition in porous electrodes remain unclear. In ZFBs, convective mass transfer is deemed to have a considerable impact on the Zn deposition as flowing electrolytes are applied to supply reactants. Yet, the interplay between transport phenomena, liquid–solid phase change, Zn deposition morphologies, and the corresponding electrochemical performance is unclear, hindering the development of effective strategies to address the Zn dendrite issue. More fundamental studies are needed to establish an in-depth understanding of the complex Zn electrodeposition process.
3. The fundamental mechanisms of electrolyte modulation for Zn dendrite suppression need further exploration. The composition of the electrolyte will have a profound impact on the electrode/electrolyte interface properties and solvation structure of Zn^{2+} ions, which play a crucial role in determining the nucleation and growth process of Zn deposition. Unfortunately, the exact aqueous environment is dynamic and rather complex, especially in the presence of dendrite inhibitors, making it extremely challenging to clarify the fundamental interplay of electrolyte species and Zn electrochemistry. To resolve this challenge, advanced characterization techniques that can probe the solvation structures should be developed along with advanced mathematical modeling in the future.
4. The role of the membrane in Zn dendrite suppression should be further explored. At present, only a few studies on membrane engineering to suppress Zn dendrites have been conducted. Considering that membranes determine the ion flux and may be in direct contact with the deposited Zn, membranes are a critical component of ZFBs to be studied to achieve dendrite-free Zn deposition. Ion selectivity, internal resistance, mechanical strength (Zn suppression capability), stability, and cost should be delicately considered.

Author Contributions: Writing—Original Draft Preparation, Z.X.; Writing—Review and Editing, Z.X. and M.W.; Funding Acquisition, M.W. All authors have read and agreed to the published version of the manuscript.

Funding: The work described in this paper was fully supported by a grant from the Research Grants Council of the Hong Kong Special Administrative Region, China (RGC Project No. 16205721).

Conflicts of Interest: The authors declare no conflict of interest.

References

1. Guangtao Cong, Y.-C.L. Strategies to Improve the Energy Density of Non-Aqueous Organic Redox Flow Batteries. *Acta Phys.-Chim. Sin.* **2022**, *38*, 2106008. [[CrossRef](#)]
2. Lou, X.; Yuan, D.; Yu, Y.; Ding, M.; Sun, Q.; Jia, C. A Cost-effective Nafion Composite Membrane as an Effective Vanadium-Ion Barrier for Vanadium Redox Flow Batteries. *Chem. Asian J.* **2020**, *15*, 2357–2363. [[CrossRef](#)] [[PubMed](#)]
3. Holdren, J.P. Energy and sustainability. *Science* **2007**, *315*, 737. [[CrossRef](#)] [[PubMed](#)]
4. Soloveichik, G.L. Flow batteries: Current status and trends. *Chem. Rev.* **2015**, *115*, 11533–11558. [[CrossRef](#)]
5. Leung, P.; Li, X.; De León, C.P.; Berlouis, L.; Low, C.J.; Walsh, F.C. Progress in redox flow batteries, remaining challenges and their applications in energy storage. *RSC Adv.* **2012**, *2*, 10125–10156. [[CrossRef](#)]
6. Wadia, C.; Albertus, P.; Srinivasan, V. Resource constraints on the battery energy storage potential for grid and transportation applications. *J. Power Sources* **2011**, *196*, 1593–1598. [[CrossRef](#)]
7. Khor, A.; Leung, P.; Mohamed, M.; Flox, C.; Xu, Q.; An, L.; Wills, R.; Morante, J.; Shah, A. Review of zinc-based hybrid flow batteries: From fundamentals to applications. *Mater. Today Energy* **2018**, *8*, 80–108. [[CrossRef](#)]
8. Yin, Y.; Yuan, Z.; Li, X. Rechargeable aqueous zinc-bromine battery: Overview and future perspective. *Phys. Chem. Chem. Phys.* **2021**, *23*, 26070–26084. [[CrossRef](#)]

9. Gong, K.; Ma, X.; Conforti, K.M.; Kuttler, K.J.; Grunewald, J.B.; Yeager, K.L.; Bazant, M.Z.; Gu, S.; Yan, Y. A zinc–iron redox-flow battery under \$100 per kWh of system capital cost. *Energy Environ. Sci.* **2015**, *8*, 2941–2945. [[CrossRef](#)]
10. Rajarathnam, G.P. The Zinc/Bromine Flow Battery: Fundamentals and Novel Materials for Technology Advancement. Ph.D. Thesis, The University of Sydney, Sydney, NSW, Australia, 2016.
11. Pistoia, G. *Electric and Hybrid Vehicles: Power Sources, Models, Sustainability, Infrastructure and the Market*; Elsevier: Amsterdam, The Netherlands, 2010.
12. Kondoh, J.; Ishii, I.; Yamaguchi, H.; Murata, A.; Otani, K.; Sakuta, K.; Higuchi, N.; Sekine, S.; Kamimoto, M. Electrical energy storage systems for energy networks. *Energy Convers. Manag.* **2000**, *41*, 1863–1874. [[CrossRef](#)]
13. Beaudin, M.; Zareipour, H.; Schellenbergblabe, A.; Rosehart, W. Energy storage for mitigating the variability of renewable electricity sources: An updated review. *Energy Sustain. Dev.* **2010**, *14*, 302–314. [[CrossRef](#)]
14. Díaz-González, F.; Sumper, A.; Gomis-Bellmunt, O.; Villafáfila-Robles, R. A review of energy storage technologies for wind power applications. *Renew. Sust. Energ. Rev.* **2012**, *16*, 2154–2171. [[CrossRef](#)]
15. Zheng, Q.; Jiang, L.; Xu, Y.; Gao, S.; Liu, T.; Qu, C.; Chen, H.; Li, X. Research Progress and Development Suggestions of Energy Storage Technology under Background of Carbon Peak and Carbon Neutrality. *Bull. Chin. Acad. Sci. (Chin. Version)* **2022**, *37*, 529–540.
16. Li, B.; Nie, Z.; Vijayakumar, M.; Li, G.; Liu, J.; Sprenkle, V.; Wang, W. Ambipolar zinc-polyiodide electrolyte for a high-energy density aqueous redox flow battery. *Nat. Commun.* **2015**, *6*, 6303. [[CrossRef](#)] [[PubMed](#)]
17. Wang, J.; Zhang, L.; Zhang, C.; Zhang, J. Effects of bismuth ion and tetrabutylammonium bromide on the dendritic growth of zinc in alkaline zincate solutions. *J. Power Sources* **2001**, *102*, 139–143. [[CrossRef](#)]
18. Yuan, Z.; Duan, Y.; Liu, T.; Zhang, H.; Li, X. Toward a low-cost alkaline zinc–iron flow battery with a polybenzimidazole custom membrane for stationary energy storage. *IScience* **2018**, *3*, 40–49. [[CrossRef](#)] [[PubMed](#)]
19. Xie, C.; Zhang, H.; Xu, W.; Wang, W.; Li, X. A Long Cycle Life, Self-Healing Zinc–Iodine Flow Battery with High Power Density. *Angew. Chem.* **2018**, *130*, 11341–11346. [[CrossRef](#)]
20. Jiang, H.; Wu, M.; Ren, Y.; Shyy, W.; Zhao, T. Towards a uniform distribution of zinc in the negative electrode for zinc bromine flow batteries. *Appl. Energy* **2018**, *213*, 366–374. [[CrossRef](#)]
21. Lee, J.-H.; Kim, R.; Kim, S.; Heo, J.; Kwon, H.; Yang, J.H.; Kim, H.-T. Dendrite-free Zn electrodeposition triggered by interatomic orbital hybridization of Zn and single vacancy carbon defects for aqueous Zn-based flow batteries. *Energy Environ. Sci.* **2020**, *13*, 2839–2848. [[CrossRef](#)]
22. Wang, S.; Yuan, C.; Chang, N.; Song, Y.; Zhang, H.; Yin, Y.; Li, X. Act in contravention: A non-planar coupled electrode design utilizing “tip effect” for ultra-high areal capacity, long cycle life zinc-based batteries. *Sci. Bull.* **2021**, *66*, 889–896. [[CrossRef](#)]
23. Wu, M.; Zhao, T.; Wei, L.; Jiang, H.; Zhang, R. Improved electrolyte for zinc–bromine flow batteries. *J. Power Sources* **2018**, *384*, 232–239. [[CrossRef](#)]
24. Kim, D.; Jeon, J. A Zn(ClO₄)₂ supporting material for highly reversible zinc–bromine electrolytes. *Bull. Korean Chem. Soc.* **2016**, *37*, 299–304. [[CrossRef](#)]
25. Bae, S.; Lee, J.; Kim, D.S. The effect of Cr³⁺-Functionalized additive in zinc–bromine flow battery. *J. Power Sources* **2019**, *413*, 167–173. [[CrossRef](#)]
26. Wu, J.; Yuan, C.; Li, T.; Yuan, Z.; Zhang, H.; Li, X. Dendrite-free zinc-based battery with high areal capacity via the region-induced deposition effect of turing membrane. *J. Am. Chem. Soc.* **2021**, *143*, 13135–13144. [[CrossRef](#)]
27. Wu, J.; Dai, Q.; Zhang, H.; Li, X. A defect-free MOF composite membrane prepared via in-situ binder-controlled restrained second-growth method for energy storage device. *Energy Stor. Mater.* **2021**, *35*, 687–694. [[CrossRef](#)]
28. Lu, W.; Li, T.; Yuan, C.; Zhang, H.; Li, X. Advanced porous composite membrane with ability to regulate zinc deposition enables dendrite-free and high-areal capacity zinc-based flow battery. *Energy Stor. Mater.* **2022**, *47*, 415–423. [[CrossRef](#)]
29. Ulaganathan, M.; Suresh, S.; Mariyappan, K.; Periasamy, P.; Pitchai, R. New zinc–vanadium (Zn–V) hybrid redox flow battery: High-voltage and energy-efficient advanced energy storage system. *ACS Sustain. Chem. Eng.* **2019**, *7*, 6053–6060. [[CrossRef](#)]
30. Xie, Z.; Su, Q.; Shi, A.; Yang, B.; Liu, B.; Chen, J.; Zhou, X.; Cai, D.; Yang, L. High performance of zinc–ferrum redox flow battery with Ac⁻/HAc buffer solution. *J. Energy Chem.* **2016**, *25*, 495–499. [[CrossRef](#)]
31. Pan, J.; Wen, Y.; Cheng, J.; Pan, J.; Bai, S.; Yang, Y. Evaluation of substrates for zinc negative electrode in acid PbO₂–Zn single flow batteries. *Chin. J. Chem. Eng.* **2016**, *24*, 529–534. [[CrossRef](#)]
32. Li, Y.; Geysens, P.; Zhang, X.; Sniekers, J.; Fransaer, J.; Binnemans, K.; Vankelecom, I.F. Cerium-containing complexes for low-cost, non-aqueous redox flow batteries (RFBs). *J. Power Sources* **2020**, *450*, 227634. [[CrossRef](#)]
33. Yu, X.; Song, Y.; Tang, A. Tailoring manganese coordination environment for a highly reversible zinc–manganese flow battery. *J. Power Sources* **2021**, *507*, 230295. [[CrossRef](#)]
34. Yang, M.; Xu, Z.; Xiang, W.; Xu, H.; Ding, M.; Li, L.; Tang, A.; Gao, R.; Zhou, G.; Jia, C. High performance and long cycle life neutral zinc–iron flow batteries enabled by zinc–bromide complexation. *Energy Storage Mater.* **2022**, *44*, 433–440. [[CrossRef](#)]
35. Xie, C.; Li, T.; Deng, C.; Song, Y.; Zhang, H.; Li, X. A highly reversible neutral zinc/manganese battery for stationary energy storage. *Energy Environ. Sci.* **2020**, *13*, 135–143. [[CrossRef](#)]
36. Yang, J.; Song, Y.; Liu, Q.; Tang, A. High-capacity zinc–iodine flow batteries enabled by a polymer–polyiodide complex cathode. *J. Mater. Chem. A* **2021**, *9*, 16093–16098. [[CrossRef](#)]

37. Tang, L.; Li, T.; Lu, W.; Li, X. Lamella-like electrode with high Br₂-entrapping capability and activity enabled by adsorption and spatial confinement effects for bromine-based flow battery. *Sci. Bull.* **2022**, *67*, 1362–1371. [CrossRef]
38. Winsberg, J.; Stolze, C.; Schwenke, A.; Muench, S.; Hager, M.D.; Schubert, U.S. Aqueous 2,2,6,6-tetramethylpiperidine-N-oxyl catholytes for a high-capacity and high current density oxygen-insensitive hybrid-flow battery. *ACS Energy Lett.* **2017**, *2*, 411–416. [CrossRef]
39. Chen, D.; Kang, C.; Duan, W.; Yuan, Z.; Li, X. A non-ionic membrane with high performance for alkaline zinc-iron flow battery. *J. Membr. Sci.* **2021**, *618*, 118585. [CrossRef]
40. Cheng, Y.; Guo, H. Interface modification of electrodes through polyethylene glycol in rechargeable zinc-nickel batteries. *Chem. Eng. Sci.* **2021**, *232*, 116372. [CrossRef]
41. Li, X.; Liu, D.; Liu, Q.; Xiang, Z. A Pyrolysis-Free Method Toward Large-Scale Synthesis of Ultra-Highly Efficient Bifunctional Oxygen Electrocatalyst for Zinc-Air Flow Batteries. *Small* **2022**, *18*, 2201197. [CrossRef]
42. Lu, W.; Xu, P.; Shao, S.; Li, T.; Zhang, H.; Li, X. Multifunctional Carbon Felt Electrode with N-Rich Defects Enables a Long-Cycle Zinc-Bromine Flow Battery with Ultrahigh Power Density. *Adv. Funct. Mater.* **2021**, *31*, 2102913. [CrossRef]
43. Yin, Y.; Wang, S.; Zhang, Q.; Song, Y.; Chang, N.; Pan, Y.; Zhang, H.; Li, X. Dendrite-free zinc deposition induced by tin-modified multifunctional 3D host for stable zinc-based flow battery. *Adv. Mater.* **2020**, *32*, 1906803. [CrossRef] [PubMed]
44. Lee, J.-N.; Do, E.; Kim, Y.; Yu, J.-S.; Kim, K.J. Development of titanium 3D mesh interlayer for enhancing the electrochemical performance of zinc–bromine flow battery. *Sci. Rep.* **2021**, *11*, 1–9. [CrossRef]
45. Zhi, L.; Li, T.; Liu, X.; Yuan, Z.; Li, X. Functional Complexed Zincate Ions Enable Dendrite-free Long Cycle Alkaline Zinc-based Flow Batteries. *Nano Energy* **2022**, *102*, 107697. [CrossRef]
46. Jian, Q.; Wu, M.; Jiang, H.; Lin, Y.; Zhao, T. A trifunctional electrolyte for high-performance zinc-iodine flow batteries. *J. Power Sources* **2021**, *484*, 229238. [CrossRef]
47. Trudgeon, D.P.; Qiu, K.; Li, X.; Mallick, T.; Taiwo, O.O.; Chakrabarti, B.; Yufit, V.; Brandon, N.P.; Crevillen-Garcia, D.; Shah, A. Screening of effective electrolyte additives for zinc-based redox flow battery systems. *J. Power Sources* **2019**, *412*, 44–54. [CrossRef]
48. Yang, J.; Yan, H.; Hao, H.; Song, Y.; Li, Y.; Liu, Q.; Tang, A. Synergetic Modulation on Solvation Structure and Electrode Interface Enables a Highly Reversible Zinc Anode for Zinc–Iron Flow Batteries. *ACS Energy Lett.* **2022**, *7*, 2331–2339. [CrossRef]
49. Hou, X.; Huang, K.; Xia, Y.; Mu, F.; Cao, H.; Xia, Y.; Wu, Y.; Lu, Y.; Wang, Y.; Xu, F. Fish-scale-like nano-porous membrane based on zeolite nanosheets for long stable zinc-based flow battery. *AIChE J.* **2022**, *68*, e17738. [CrossRef]
50. Hu, J.; Yue, M.; Zhang, H.; Yuan, Z.; Li, X. A Boron Nitride Nanosheets Composite Membrane for a Long-Life Zinc-Based Flow Battery. *Angew. Chem. Int. Ed.* **2020**, *59*, 6715–6719. [CrossRef]
51. Chang, N.; Yin, Y.; Yue, M.; Yuan, Z.; Zhang, H.; Lai, Q.; Li, X. A Cost-Effective Mixed Matrix Polyethylene Porous Membrane for Long-Cycle High Power Density Alkaline Zinc-Based Flow Batteries. *Adv. Funct. Mater.* **2019**, *29*, 1901674. [CrossRef]
52. Jeena, C.B.; Elsa, P.J.; Moly, P.P.; Ambily, K.J.; Joy, V.T. A dendrite free Zn-Fe hybrid redox flow battery for renewable energy storage. *Energy Stor.* **2022**, *4*, e275. [CrossRef]
53. Zuo, Y.; Wang, K.; Pei, P.; Wei, M.; Liu, X.; Xiao, Y.; Zhang, P. Zinc dendrite growth and inhibition strategies. *Mater. Today Energy* **2021**, *20*, 100692. [CrossRef]
54. Mitha, A.; Yazdi, A.Z.; Ahmed, M.; Chen, P. Surface adsorption of polyethylene glycol to suppress dendrite formation on zinc anodes in rechargeable aqueous batteries. *ChemElectroChem* **2018**, *5*, 2409–2418. [CrossRef]
55. Xu, M.; Ivey, D.; Qu, W.; Xie, Z. Study of the mechanism for electrodeposition of dendrite-free zinc in an alkaline electrolyte modified with 1-ethyl-3-methylimidazolium dicyanamide. *J. Power Sources* **2015**, *274*, 1249–1253. [CrossRef]
56. Cheng, Y.; Xi, X.; Li, D.; Li, X.; Lai, Q.; Zhang, H. Performance and potential problems of high power density zinc–nickel single flow batteries. *RSC Adv.* **2015**, *5*, 1772–1776. [CrossRef]
57. Lu, W.; Xie, C.; Zhang, H.; Li, X. Inhibition of zinc dendrite growth in zinc-based batteries. *ChemSusChem* **2018**, *11*, 3996–4006. [CrossRef]
58. Yang, Q.; Liang, G.; Guo, Y.; Liu, Z.; Yan, B.; Wang, D.; Huang, Z.; Li, X.; Fan, J.; Zhi, C. Do zinc dendrites exist in neutral zinc batteries: A developed electrohealing strategy to in situ rescue in-service batteries. *Adv. Mater.* **2019**, *31*, 1903778. [CrossRef] [PubMed]
59. Xie, C.; Li, Y.; Wang, Q.; Sun, D.; Tang, Y.; Wang, H. Issues and solutions toward zinc anode in aqueous zinc-ion batteries: A mini review. *Carbon Energy* **2020**, *2*, 540–560. [CrossRef]
60. Zeng, Y.; Zhang, X.; Qin, R.; Liu, X.; Fang, P.; Zheng, D.; Tong, Y.; Lu, X. Dendrite-free zinc deposition induced by multifunctional CNT frameworks for stable flexible Zn-ion batteries. *Adv. Mater.* **2019**, *31*, 1903675. [CrossRef]
61. Hao, J.; Li, X.; Zeng, X.; Li, D.; Mao, J.; Guo, Z. Deeply understanding the Zn anode behaviour and corresponding improvement strategies in different aqueous Zn-based batteries. *Energy Environ. Sci.* **2020**, *13*, 3917–3949. [CrossRef]
62. Xu, C.; Li, B.; Du, H.; Kang, F. Energetic zinc ion chemistry: The rechargeable zinc ion battery. *Angew. Chem.* **2012**, *124*, 957–959. [CrossRef]
63. Han, C.; Li, W.; Liu, H.K.; Dou, S.; Wang, J. Principals and strategies for constructing a highly reversible zinc metal anode in aqueous batteries. *Nano Energy* **2020**, *74*, 104880. [CrossRef]
64. Kundu, D.; Adams, B.D.; Duffort, V.; Vajargah, S.H.; Nazar, L.F. A high-capacity and long-life aqueous rechargeable zinc battery using a metal oxide intercalation cathode. *Nat. Energy* **2016**, *1*, 16119. [CrossRef]

65. Wang, F.; Borodin, O.; Gao, T.; Fan, X.; Sun, W.; Han, F.; Faraone, A.; Dura, J.A.; Xu, K.; Wang, C. Highly reversible zinc metal anode for aqueous batteries. *Nat. Mater.* **2018**, *17*, 543–549. [CrossRef] [PubMed]
66. Shaigan, N.; Qu, W.; Takeda, T. Morphology control of electrodeposited zinc from alkaline zincate solutions for rechargeable zinc air batteries. *ECS Trans.* **2010**, *28*, 35. [CrossRef]
67. Pan, H.; Shao, Y.; Yan, P.; Cheng, Y.; Han, K.S.; Nie, Z.; Wang, C.; Yang, J.; Li, X.; Bhattacharya, P. Reversible aqueous zinc/manganese oxide energy storage from conversion reactions. *Nat. Energy* **2016**, *1*, 16039. [CrossRef]
68. Stamm, J.; Varzi, A.; Latz, A.; Horstmann, B. Modeling nucleation and growth of zinc oxide during discharge of primary zinc-air batteries. *J. Power Sources* **2017**, *360*, 136–149. [CrossRef]
69. Zhang, Q.; Luan, J.; Tang, Y.; Ji, X.; Wang, H. Interfacial design of dendrite-free zinc anodes for aqueous zinc-ion batteries. *Angew. Chem. Int. Ed.* **2020**, *59*, 13180–13191. [CrossRef]
70. Pei, A.; Zheng, G.; Shi, F.; Li, Y.; Cui, Y. Nanoscale nucleation and growth of electrodeposited lithium metal. *Nano Lett.* **2017**, *17*, 1132–1139. [CrossRef]
71. Yang, J.L.; Li, J.; Zhao, J.W.; Liu, K.; Yang, P.; Fan, H.J. Stable Zinc Anode Enabled by Zincophilic Polyanionic Hydrogel Layer. *Adv. Mater.* **2022**, *34*, 2202382. [CrossRef]
72. Zhao, Z.; Zhao, J.; Hu, Z.; Li, J.; Li, J.; Zhang, Y.; Wang, C.; Cui, G. Long-life and deeply rechargeable aqueous Zn anodes enabled by a multifunctional brightener-inspired interphase. *Energy Environ. Sci.* **2019**, *12*, 1938–1949. [CrossRef]
73. Li, C.; Shyamsunder, A.; Hoane, A.G.; Long, D.M.; Kwok, C.Y.; Kotula, P.G.; Zavadil, K.R.; Gewirth, A.A.; Nazar, L.F. Highly reversible Zn anode with a practical areal capacity enabled by a sustainable electrolyte and superacid interfacial chemistry. *Joule* **2022**, *6*, 1103–1120. [CrossRef]
74. Cui, B.-F.; Han, X.-P.; Hu, W.-B. Micronanostructured design of dendrite-free zinc anodes and their applications in aqueous zinc-based rechargeable batteries. *Small Struct.* **2021**, *2*, 2000128. [CrossRef]
75. Gunawardena, G.; Hills, G.; Montenegro, I.; Scharifker, B. Electrochemical nucleation: Part I. general considerations. *J. Electroanal. Chem. Interfacial Electrochem.* **1982**, *138*, 225–239. [CrossRef]
76. Guo, L.; Guo, H.; Huang, H.; Tao, S.; Cheng, Y. Inhibition of zinc dendrites in zinc-based flow batteries. *Front. Chem.* **2020**, *8*, 557. [CrossRef] [PubMed]
77. Cao, Q.; Gao, H.; Gao, Y.; Yang, J.; Li, C.; Pu, J.; Du, J.; Yang, J.; Cai, D.; Pan, Z. Regulating dendrite-free zinc deposition by 3D zincophilic nitrogen-doped vertical graphene for high-performance flexible Zn-ion batteries. *Adv. Funct. Mater.* **2021**, *31*, 2103922. [CrossRef]
78. Wu, C.; Xie, K.; Ren, K.; Yang, S.; Wang, Q. Dendrite-free Zn anodes enabled by functional nitrogen-doped carbon protective layers for aqueous zinc-ion batteries. *Dalton Trans.* **2020**, *49*, 17629–17634. [CrossRef]
79. Jian, Q.; Guo, Z.; Zhang, L.; Wu, M.; Zhao, T. A hierarchical porous tin host for dendrite-free, highly reversible zinc anodes. *Chem. Eng. J.* **2021**, *425*, 130643. [CrossRef]
80. Yufit, V.; Tariq, F.; Eastwood, D.S.; Biton, M.; Wu, B.; Lee, P.D.; Brandon, N.P. Operando visualization and multi-scale tomography studies of dendrite formation and dissolution in zinc batteries. *Joule* **2019**, *3*, 485–502. [CrossRef]
81. Trudgeon, D.P.; Li, X. The effect of electrolyte and additive concentration on zinc–nickel flow cell performance. *Electrochim. Acta* **2021**, *367*, 137479. [CrossRef]
82. Walsh, F.C.; Ponce de Léon, C.; Berlouis, L.; Nikiforidis, G.; Arenas-Martínez, L.F.; Hodgson, D.; Hall, D. The development of Zn–Ce hybrid redox flow batteries for energy storage and their continuing challenges. *ChemPlusChem* **2015**, *80*, 288–311. [CrossRef]
83. Rajarathnam, G.P.; Schneider, M.; Sun, X.; Vassallo, A.M. The influence of supporting electrolytes on zinc half-cell performance in zinc/bromine flow batteries. *J. Electrochem. Soc.* **2015**, *163*, A5112. [CrossRef]
84. Zheng, J.; Yin, J.; Zhang, D.; Li, G.; Bock, D.C.; Tang, T.; Zhao, Q.; Liu, X.; Warren, A.; Deng, Y. Spontaneous and field-induced crystallographic reorientation of metal electrodeposits at battery anodes. *Sci. Adv.* **2020**, *6*, eabb1122. [CrossRef] [PubMed]
85. Wang, S.; Wang, Z.; Yin, Y.; Li, T.; Chang, N.; Fan, F.; Zhang, H.; Li, X. A highly reversible zinc deposition for flow batteries regulated by critical concentration induced nucleation. *Energy Environ. Sci.* **2021**, *14*, 4077–4084. [CrossRef]
86. Wang, S.; Li, T.; Yin, Y.; Chang, N.; Zhang, H.; Li, X. High-energy-density aqueous zinc-based hybrid supercapacitor-battery with uniform zinc deposition achieved by multifunctional decoupled additive. *Nano Energy* **2022**, *96*, 107120. [CrossRef]
87. Xu, P.; Li, T.; Zheng, Q.; Zhang, H.; Yin, Y.; Li, X. A low-cost bromine-fixed additive enables a high capacity retention zinc-bromine batteries. *J. Energy Chem.* **2022**, *65*, 89–93. [CrossRef]
88. Turney, D.E.; Gallaway, J.W.; Yadav, G.G.; Ramirez, R.; Nyce, M.; Banerjee, S.; Chen-Wiegart, Y.-C.K.; Wang, J.; D'Ambrose, M.J.; Kolhekar, S. Rechargeable zinc alkaline anodes for long-cycle energy storage. *Chem. Mater.* **2017**, *29*, 4819–4832. [CrossRef]
89. Yang, H.S.; Park, J.H.; Ra, H.W.; Jin, C.-S.; Yang, J.H. Critical rate of electrolyte circulation for preventing zinc dendrite formation in a zinc–bromine redox flow battery. *J. Power Sources* **2016**, *325*, 446–452. [CrossRef]
90. Moshtev, R.; Zlatilova, P. Kinetics of growth of zinc dendrite precursors in zincate solutions. *J. Appl. Electrochem.* **1978**, *8*, 213–222. [CrossRef]
91. Ito, Y.; Nyce, M.; Plivelich, R.; Klein, M.; Steingart, D.; Banerjee, S. Zinc morphology in zinc–nickel flow assisted batteries and impact on performance. *J. Power Sources* **2011**, *196*, 2340–2345. [CrossRef]
92. Wang, G.; Zou, H.; Xu, Z.; Tang, A.; Zhong, F.; Zhu, X.; Qin, C.; Ding, M.; You, W.; Jia, C. Unlocking the solubility limit of ferrocyanide for high energy density redox flow batteries. *Mater. Today Energy* **2022**, *28*, 101061. [CrossRef]

93. Han, D.; Shanmugam, S. Active material crossover suppression with bi-ionic transportability by an amphoteric membrane for Zinc–Bromine redox flow battery. *J. Power Sources* **2022**, *540*, 231637. [\[CrossRef\]](#)
94. Chu, F.; Guo, L.; Wang, S.; Cheng, Y. Semi-solid zinc slurry with abundant electron-ion transfer interfaces for aqueous zinc-based flow batteries. *J. Power Sources* **2022**, *535*, 231442. [\[CrossRef\]](#)
95. Zeng, Y.; Zhou, X.; An, L.; Wei, L.; Zhao, T. A high-performance flow-field structured iron-chromium redox flow battery. *J. Power Sources* **2016**, *324*, 738–744. [\[CrossRef\]](#)
96. Deng, Q.; Huang, P.; Zhou, W.X.; Ma, Q.; Zhou, N.; Xie, H.; Ling, W.; Zhou, C.J.; Yin, Y.X.; Wu, X.W. A high-performance composite electrode for vanadium redox flow batteries. *Adv. Energy Mater.* **2017**, *7*, 1700461. [\[CrossRef\]](#)
97. Leung, P.; Mohamed, M.; Shah, A.; Xu, Q.; Conde-Duran, M. A mixed acid based vanadium–cerium redox flow battery with a zero-gap serpentine architecture. *J. Power Sources* **2015**, *274*, 651–658. [\[CrossRef\]](#)
98. Yuan, Z.; Yin, Y.; Xie, C.; Zhang, H.; Yao, Y.; Li, X. Advanced materials for zinc-based flow battery: Development and challenge. *Adv. Mater.* **2019**, *31*, 1902025. [\[CrossRef\]](#)
99. Narayanan, N.V.; Ashokraj, B.; Sampath, S. Ambient temperature, zinc ion-conducting, binary molten electrolyte based on acetamide and zinc perchlorate: Application in rechargeable zinc batteries. *J. Colloid Interface Sci.* **2010**, *342*, 505–512. [\[CrossRef\]](#)
100. Chang, N.; Li, T.; Li, R.; Wang, S.; Yin, Y.; Zhang, H.; Li, X. An aqueous hybrid electrolyte for low-temperature zinc-based energy storage devices. *Energy Environ. Sci.* **2020**, *13*, 3527–3535. [\[CrossRef\]](#)
101. Dyshin, A.A.; Eliseeva, O.V.; Kiselev, M.G. Density and Viscosity of Zinc Chloride Solution in N-Methylacetamide over the Temperature Range from 308.15 to 328.15 K at Atmospheric Pressure. *J. Chem. Eng. Data* **2018**, *63*, 3130–3135. [\[CrossRef\]](#)
102. Li, X.; Wang, H.; Sun, X.; Li, J.; Liu, Y.-N. Flexible wide-temperature zinc-ion battery enabled by an ethylene glycol-based organohydrogel electrolyte. *ACS Appl. Energy Mater.* **2021**, *4*, 12718–12727. [\[CrossRef\]](#)
103. Nikiforidis, G.; Berlouis, L.; Hall, D.; Hodgson, D. A study of different carbon composite materials for the negative half-cell reaction of the zinc cerium hybrid redox flow cell. *Electrochim. Acta* **2013**, *113*, 412–423. [\[CrossRef\]](#)
104. Afifi, S.; Ebaid, A.; Hegazy, M.; Donya, K. On the electrowinning of zinc from alkaline zincate solutions. *J. Electrochem. Soc.* **1991**, *138*, 1929. [\[CrossRef\]](#)
105. Guo, Y.; Li, D.; Xiong, R.; Li, H. Investigation of the temperature-dependent behaviours of Li metal anode. *Chem. Commun.* **2019**, *55*, 9773–9776. [\[CrossRef\]](#) [\[PubMed\]](#)
106. Yan, K.; Wang, J.; Zhao, S.; Zhou, D.; Sun, B.; Cui, Y.; Wang, G. Temperature-dependent Nucleation and Growth of Dendrite-free Lithium Metal Anodes. *Angew. Chem.* **2019**, *131*, 11486–11490. [\[CrossRef\]](#)
107. Leung, P.; Ponce-de-León, C.; Low, C.; Walsh, F. Zinc deposition and dissolution in methanesulfonic acid onto a carbon composite electrode as the negative electrode reactions in a hybrid redox flow battery. *Electrochim. Acta* **2011**, *56*, 6536–6546. [\[CrossRef\]](#)
108. Galvani, F.; Carlos, I.A. The effect of the additive glycerol on zinc electrodeposition on steel. *Met. Finish.* **1997**, *95*, 70–72. [\[CrossRef\]](#)
109. Leung, P.; Ponce-de-León, C.; Recio, F.; Herrasti, P.; Walsh, F. Corrosion of the zinc negative electrode of zinc–cerium hybrid redox flow batteries in methanesulfonic acid. *J. Appl. Electrochem.* **2014**, *44*, 1025–1035. [\[CrossRef\]](#)
110. Lim, H.; Lackner, A.; Knechtli, R. Zinc–bromine secondary battery. *J. Electrochem. Soc.* **1977**, *124*, 1154. [\[CrossRef\]](#)
111. Hao, J.; Li, X.; Zhang, S.; Yang, F.; Zeng, X.; Zhang, S.; Bo, G.; Wang, C.; Guo, Z. Designing dendrite-free zinc anodes for advanced aqueous zinc batteries. *Adv. Funct. Mater.* **2020**, *30*, 2001263. [\[CrossRef\]](#)
112. Lu, W.; Zhang, C.; Zhang, H.; Li, X. Anode for zinc-based batteries: Challenges, strategies, and prospects. *ACS Energy Lett.* **2021**, *6*, 2765–2785. [\[CrossRef\]](#)
113. Gabe, D. The role of hydrogen in metal electrodeposition processes. *J. Appl. Electrochem.* **1997**, *27*, 908–915. [\[CrossRef\]](#)
114. Ganne, F.; Cachet, C.; Maurin, G.; Wiart, R.; Chauveau, E.; Petitjean, J. Impedance spectroscopy and modelling of zinc deposition in chloride electrolyte containing a commercial additive. *J. Appl. Electrochem.* **2000**, *30*, 665–673. [\[CrossRef\]](#)
115. Thomas, S.; Birbilis, N.; Venkatraman, M.; Cole, I. Corrosion of zinc as a function of pH. *Corros., J. Sci. Eng.* **2012**, *68*, 015009–015001–015009. [\[CrossRef\]](#)
116. Bayaguud, A.; Fu, Y.; Zhu, C. Interfacial parasitic reactions of zinc anodes in zinc ion batteries: Underestimated corrosion and hydrogen evolution reactions and their suppression strategies. *J. Energy Chem.* **2022**, *64*, 246–262. [\[CrossRef\]](#)
117. Ma, L.; Li, Q.; Ying, Y.; Ma, F.; Chen, S.; Li, Y.; Huang, H.; Zhi, C. Toward practical high-areal-capacity aqueous zinc-metal batteries: Quantifying hydrogen evolution and a solid-ion conductor for stable zinc anodes. *Adv. Mater.* **2021**, *33*, 2007406. [\[CrossRef\]](#) [\[PubMed\]](#)
118. Yuan, X.; Mo, J.; Huang, J.; Liu, J.; Liu, C.; Zeng, X.; Zhou, W.; Yue, J.; Wu, X.; Wu, Y. An Aqueous Hybrid Zinc–Bromine Battery with High Voltage and Energy Density. *ChemElectroChem* **2020**, *7*, 1531–1536. [\[CrossRef\]](#)
119. Zhu, M.; Hu, J.; Lu, Q.; Dong, H.; Karnaushenko, D.D.; Becker, C.; Karnaushenko, D.; Li, Y.; Tang, H.; Qu, Z. A patternable and in situ formed polymeric zinc blanket for a reversible zinc anode in a skin-mountable microbattery. *Adv. Mater.* **2021**, *33*, 2007497. [\[CrossRef\]](#)
120. Hao, J.; Li, B.; Li, X.; Zeng, X.; Zhang, S.; Yang, F.; Liu, S.; Li, D.; Wu, C.; Guo, Z. An in-depth study of Zn metal surface chemistry for advanced aqueous Zn-ion batteries. *Adv. Mater.* **2020**, *32*, 2003021. [\[CrossRef\]](#)
121. Yang, J.; Yin, B.; Sun, Y.; Pan, H.; Sun, W.; Jia, B.; Zhang, S.; Ma, T. Zinc anode for mild aqueous zinc-ion batteries: Challenges, strategies, and perspectives. *Nano-Micro Lett.* **2022**, *14*, 1–47. [\[CrossRef\]](#)

122. Alfantazi, A.; Dreisinger, D. The role of zinc and sulfuric acid concentrations on zinc electrowinning from industrial sulfate based electrolyte. *J. Appl. Electrochem.* **2001**, *31*, 641–646. [CrossRef]
123. Yan, Y.; Shu, C.; Zeng, T.; Wen, X.; Liu, S.; Deng, D.; Zeng, Y. Surface-Preferred Crystal Plane Growth Enabled by Underpotential Deposited Monolayer toward Dendrite-Free Zinc Anode. *ACS Nano* **2022**, *16*, 9150–9162. [CrossRef] [PubMed]
124. Zheng, J.; Zhao, Q.; Tang, T.; Yin, J.; Quilty, C.D.; Renderos, G.D.; Liu, X.; Deng, Y.; Wang, L.; Bock, D.C. Reversible epitaxial electrodeposition of metals in battery anodes. *Science* **2019**, *366*, 645–648. [CrossRef] [PubMed]
125. Wang, G.; Kohn, B.; Scheler, U.; Wang, F.; Oswald, S.; Löffler, M.; Tan, D.; Zhang, P.; Zhang, J.; Feng, X. A High-Voltage, Dendrite-Free, and Durable Zn–Graphite Battery. *Adv. Mater.* **2020**, *32*, 1905681. [CrossRef] [PubMed]
126. Pu, S.D.; Gong, C.; Tang, Y.T.; Ning, Z.; Liu, J.; Zhang, S.; Yuan, Y.; Melvin, D.; Yang, S.; Pi, L. Achieving Ultra-High Rate Planar and Dendrite-Free Zinc Electroplating for Aqueous Zinc Battery Anodes. *Adv. Mater.* **2022**, *34*, 2202552. [CrossRef] [PubMed]
127. Su, T.T.; Wang, K.; Chi, B.Y.; Ren, W.F.; Sun, R.C. Stripy zinc array with preferential crystal plane for the ultra-long lifespan of zinc metal anodes for zinc ion batteries. *EcoMat* **2022**, e12219. [CrossRef]
128. Youssef, K.M.; Koch, C.; Fedkiw, P. Influence of additives and pulse electrodeposition parameters on production of nanocrystalline zinc from zinc chloride electrolytes. *J. Electrochem. Soc.* **2004**, *151*, C103. [CrossRef]
129. Gomes, A.; da Silva Pereira, M. Pulsed electrodeposition of Zn in the presence of surfactants. *Electrochim. Acta* **2006**, *51*, 1342–1350. [CrossRef]
130. Youssef, K.M.; Koch, C.; Fedkiw, P. Improved corrosion behavior of nanocrystalline zinc produced by pulse-current electrodeposition. *Corros. Sci.* **2004**, *46*, 51–64. [CrossRef]
131. Saber, K.; Koch, C.; Fedkiw, P. Pulse current electrodeposition of nanocrystalline zinc. *Mater. Sci. Eng. A* **2003**, *341*, 174–181. [CrossRef]
132. Kavitha, B.; Santhosh, P.; Renukadevi, M.; Kalpana, A.; Shakkthivel, P.; Vasudevan, T. Role of organic additives on zinc plating. *Surf. Coat. Technol.* **2006**, *201*, 3438–3442. [CrossRef]
133. Yu, H.; Chen, Y.; Wang, H.; Ni, X.; Wei, W.; Ji, X.; Chen, L. Engineering multi-functionalized molecular skeleton layer for dendrite-free and durable zinc batteries. *Nano Energy* **2022**, *99*, 107426. [CrossRef]
134. Di, S.; Nie, X.; Ma, G.; Yuan, W.; Wang, Y.; Liu, Y.; Shen, S.; Zhang, N. Zinc anode stabilized by an organic-inorganic hybrid solid electrolyte interphase. *Energy Stor. Mater.* **2021**, *43*, 375–382. [CrossRef]
135. Sun, K.E.; Hoang, T.K.; Doan, T.N.L.; Yu, Y.; Chen, P. Highly sustainable zinc anodes for a rechargeable hybrid aqueous battery. *Chem. Eur. J.* **2018**, *24*, 1667–1673. [CrossRef]
136. Yuan, L.; Hao, J.; Kao, C.-C.; Wu, C.; Liu, H.-K.; Dou, S.-X.; Qiao, S.-Z. Regulation methods for the Zn/electrolyte interphase and the effectiveness evaluation in aqueous Zn-ion batteries. *Energy Environ. Sci.* **2021**, *14*, 5669–5689. [CrossRef]
137. Otani, T.; Okuma, T.; Homma, T. Effect of indium and tin additives on the surface morphology of zinc negative electrodes for Zn-Ni flow-assisted batteries. *J. Electroanal. Chem.* **2020**, *878*, 114583. [CrossRef]
138. Bockelmann, M.; Kunz, U.; Turek, T. Electrically rechargeable zinc-oxygen flow battery with high power density. *Electrochim. Commun.* **2016**, *69*, 24–27. [CrossRef]
139. Nikiforidis, G.; Daoud, W.A. Indium modified graphite electrodes on highly zinc containing methanesulfonate electrolyte for zinc-cerium redox flow battery. *Electrochim. Acta* **2015**, *168*, 394–402. [CrossRef]
140. Elrouby, M.; Shilkamy, H.A.E.S.; Elsayed, A. Development of the electrochemical performance of zinc via alloying with indium as anode for alkaline batteries application. *J. Alloys Compd.* **2021**, *854*, 157285. [CrossRef]
141. Sun, P.; Ma, L.; Zhou, W.; Qiu, M.; Wang, Z.; Chao, D.; Mai, W. Simultaneous regulation on solvation shell and electrode interface for dendrite-free Zn ion batteries achieved by a low-cost glucose additive. *Angew. Chem.* **2021**, *133*, 18395–18403. [CrossRef]
142. Zhang, T.; Tang, Y.; Guo, S.; Cao, X.; Pan, A.; Fang, G.; Zhou, J.; Liang, S. Fundamentals and perspectives in developing zinc-ion battery electrolytes: A comprehensive review. *Energy Environ. Sci.* **2020**, *13*, 4625–4665. [CrossRef]
143. Li, C.; Xie, X.; Liang, S.; Zhou, J. Issues and future perspective on zinc metal anode for rechargeable aqueous zinc-ion batteries. *Energy Environ. Mater.* **2020**, *3*, 146–159. [CrossRef]
144. Suresh, S.; Kesavan, T.; Munaiah, Y.; Arulraj, I.; Dheenadayalan, S.; Ragupathy, P. Zinc–bromine hybrid flow battery: Effect of zinc utilization and performance characteristics. *RSC Adv.* **2014**, *4*, 37947–37953. [CrossRef]
145. Durmus, Y.E.; Montiel Guerrero, S.S.; Tempel, H.; Hausen, F.; Kungl, H.; Eichel, R.-A. Influence of Al alloying on the electrochemical behavior of Zn electrodes for Zn–Air batteries with neutral sodium chloride electrolyte. *Front. Chem.* **2019**, *7*, 800. [CrossRef]
146. Chang, S.; Ye, J.; Zhou, W.; Wu, C.; Ding, M.; Long, Y.; Cheng, Y.; Jia, C. A low-cost SPEEK-K type membrane for neutral aqueous zinc-iron redox flow battery. *Surf. Coat. Technol.* **2019**, *358*, 190–194. [CrossRef]
147. Xie, C.; Duan, Y.; Xu, W.; Zhang, H.; Li, X. A Low-Cost Neutral Zinc–Iron Flow Battery with High Energy Density for Stationary Energy Storage. *Angew. Chem. Int. Ed.* **2017**, *56*, 14953–14957. [CrossRef]
148. Pan, J.; Wen, Y.; Cheng, J.; Pan, J.; Bai, Z.; Yang, Y. Zinc deposition and dissolution in sulfuric acid onto a graphite–resin composite electrode as the negative electrode reactions in acidic zinc-based redox flow batteries. *J. Appl. Electrochem.* **2013**, *43*, 541–551. [CrossRef]
149. Banik, S.J.; Akolkar, R. Suppressing dendrite growth during zinc electrodeposition by PEG-200 additive. *J. Electrochem. Soc.* **2013**, *160*, D519. [CrossRef]

150. Banik, S.J.; Akolkar, R. Suppressing dendritic growth during alkaline zinc electrodeposition using polyethylenimine additive. *Electrochim. Acta* **2015**, *179*, 475–481. [[CrossRef](#)]
151. Xu, W.; Zhao, K.; Huo, W.; Wang, Y.; Yao, G.; Gu, X.; Cheng, H.; Mai, L.; Hu, C.; Wang, X. Diethyl ether as self-healing electrolyte additive enabled long-life rechargeable aqueous zinc ion batteries. *Nano Energy* **2019**, *62*, 275–281. [[CrossRef](#)]
152. Ghavami, R.K.; Rafiei, Z. Performance improvements of alkaline batteries by studying the effects of different kinds of surfactant and different derivatives of benzene on the electrochemical properties of electrolytic zinc. *J. Power Sources* **2006**, *162*, 893–899. [[CrossRef](#)]
153. Hosseini, S.; Han, S.J.; Arponwichanop, A.; Yonezawa, T.; Kheawhom, S. Ethanol as an electrolyte additive for alkaline zinc-air flow batteries. *Sci. Rep.* **2018**, *8*, 1–11. [[CrossRef](#)] [[PubMed](#)]
154. Zhou, H.; Huang, Q.; Liang, M.; Lv, D.; Xu, M.; Li, H.; Li, W. Investigation on synergism of composite additives for zinc corrosion inhibition in alkaline solution. *Mater. Chem. Phys.* **2011**, *128*, 214–219. [[CrossRef](#)]
155. Xu, Z.; Fan, Q.; Li, Y.; Wang, J.; Lund, P.D. Review of zinc dendrite formation in zinc bromine redox flow battery. *Renew. Sust. Energ. Rev.* **2020**, *127*, 109838. [[CrossRef](#)]
156. Xu, Y.; Zhu, J.; Feng, J.; Wang, Y.; Wu, X.; Ma, P.; Zhang, X.; Wang, G.; Yan, X. A rechargeable aqueous zinc/sodium manganese oxides battery with robust performance enabled by Na₂SO₄ electrolyte additive. *Energy Stor. Mater.* **2021**, *38*, 299–308. [[CrossRef](#)]
157. Wu, M.; Jiang, H.; Zhang, R.; Wei, L.; Chan, K.Y.; Zhao, T. N-doped graphene nanoplatelets as a highly active catalyst for Br₂/Br[−] redox reactions in zinc-bromine flow batteries. *Electrochim. Acta* **2019**, *318*, 69–75. [[CrossRef](#)]
158. Kim, R.; Yuk, S.; Lee, J.-H.; Choi, C.; Kim, S.; Heo, J.; Kim, H.-T. Scaling the water cluster size of Nafion membranes for a high performance Zn/Br redox flow battery. *J. Membr. Sci.* **2018**, *564*, 852–858. [[CrossRef](#)]
159. Lai, Q.; Zhang, H.; Li, X.; Zhang, L.; Cheng, Y. A novel single flow zinc–bromine battery with improved energy density. *J. Power Sources* **2013**, *235*, 1–4. [[CrossRef](#)]
160. Yuan, Z.; Liang, L.; Dai, Q.; Li, T.; Song, Q.; Zhang, H.; Hou, G.; Li, X. Low-cost hydrocarbon membrane enables commercial-scale flow batteries for long-duration energy storage. *Joule* **2022**, *6*, 884–905. [[CrossRef](#)]
161. Xie, C.; Liu, Y.; Lu, W.; Zhang, H.; Li, X. Highly stable zinc–iodine single flow batteries with super high energy density for stationary energy storage. *Energy Environ. Sci.* **2019**, *12*, 1834–1839. [[CrossRef](#)]
162. Yuan, Z.; Liu, X.; Xu, W.; Duan, Y.; Zhang, H.; Li, X. Negatively charged nanoporous membrane for a dendrite-free alkaline zinc-based flow battery with long cycle life. *Nat. Commun.* **2018**, *9*, 1–11. [[CrossRef](#)]
163. Hu, J.; Yuan, C.; Zhi, L.; Zhang, H.; Yuan, Z.; Li, X. In Situ Defect-Free Vertically Aligned Layered Double Hydroxide Composite Membrane for High Areal Capacity and Long-Cycle Zinc-Based Flow Battery. *Adv. Funct. Mater.* **2021**, *31*, 2102167. [[CrossRef](#)]